

# Priority Choice Experimental Two-qubit Tomography: Measuring One by One All Elements of Density Matrices

Karol Bartkiewicz,<sup>1,2,\*</sup> Antonín Černoč,<sup>2,3</sup> Karel Lemr,<sup>2</sup> and Adam Miranowicz<sup>4,1</sup>

<sup>1</sup>*Faculty of Physics, Adam Mickiewicz University, PL-61-614 Poznań, Poland*

<sup>2</sup>*RCPTM, Joint Laboratory of Optics of Palacký University and Institute of Physics of Academy of Sciences of the Czech Republic, 17. listopadu 12, 772 07 Olomouc, Czech Republic*

<sup>3</sup>*Institute of Physics of Academy of Science of the Czech Republic, Joint Laboratory of Optics of Palacký University and Institute of Physics of Academy of Sciences of the Czech Republic, 17. listopadu 50A, 77207 Olomouc, Czech Republic*

<sup>4</sup>*CEMS, RIKEN, 351-0198 Wako-shi, Japan*

In standard optical tomographic methods, the off-diagonal elements of a density matrix  $\rho$  are measured indirectly. Thus, the reconstruction of  $\rho$ , even if it is based on linear inversion, typically magnifies small errors in the experimental data. Recently, an optimal tomography [Phys. Rev. A **90**, 062123 (2014)] has been proposed theoretically to measure one-by-one all the elements of  $\rho$ . Thus, the relative errors in the reconstructed state can be the same as those in the experimental data. We implemented this method for two-qubit polarization states performing both local and global measurements. For comparison, we also experimentally implemented other well-known tomographic protocols based solely on local measurements (of, e.g., the Pauli operators and James-Kwiat-Munro-White projectors) and those with mutually unbiased bases requiring both local and global measurements. We reconstructed seventeen of two-qubit polarization states including separable, partially and maximally entangled. Our experiments show the highest stability against errors of our method in comparison to the other quantum tomographies. In particular, we demonstrate that each optimally-reconstructed state is embedded in the uncertainty circle of the smallest radius, both in terms of the trace distance and disturbance. We explain how to estimate experimentally the uncertainty radii for all the implemented tomographies and show that, for each reconstructed state, the relevant uncertainty circles intersect indicating the approximate location of the corresponding physical density matrix.

PACS numbers: 03.65.Wj, 03.67.-a, 42.50.Ex

*Introduction.*— Quantum tomographic methods are indispensable tools in experimental quantum physics. Indeed, characterizing quantum states and quantum processes are essential problems in studying the performance and evolution of quantum systems [1] and in developing quantum technologies [2]. Moreover, both these problems are mathematically equivalent and are usually solved by applying quantum state tomography (QST). This approach is typically based on linear inversion [3] and maximum-likelihood estimation [4–14]. There are also other proposals of quantum state estimation based on, e.g., least-squares inversion [15] as well as Bayesian mean estimation [1, 16, 17], or linear regression estimation [18]. There exist dozens of QST protocols even in the special case of reconstructing the photonic polarization states (for a review see Ref. [19] and also, e.g., Refs. [20–28]). Thus, choosing the best of them appeared to be not a simple task. However, a recent paper [29] describes an optimal QST protocol that minimizes the condition number  $\kappa$  that characterizes the robustness against experimental errors. Condition numbers were also used for investigating the error stability of optical tomographic protocols in Refs. [21, 30, 31]. In this Letter we experimentally study this optimal protocol in comparison to four other popular approaches using the same experimental setup for the reconstruction of two polarization-

entangled photons. These protocols include those based solely on the local measurements of (i) the James-Kwiat-Munro-White (JKMW) projectors [4], (ii) the Pauli operators, and (iii) their eigenstates (the so-called standard basis) [20, 32], together with (iv) the protocol of Adamson and Steinberg [22] based on mutually-unbiased bases (MUB) and applying both local and global measurements, analogously to the optimal protocol. To compare these protocols we first derive a relation between the radius of an error circle associated with the reconstructed state and measured quantities. The radii correspond to the trace distance between the ideal density matrices and the reconstructed noisy ones. However, they can also be interpreted in terms of fidelity (or disturbance).

All the approaches analyzed here are based on solving a linear-system problem  $Ax = b$ , where  $A$  is referred to as the *coefficient matrix*,  $b$  is the *observation vector* containing the measured data, and  $x = \text{vec}(\rho)$  is a real vector describing the unknown state  $\rho$  to be reconstructed. Here we choose

$$x = \text{vec}(\rho) = [\rho_{11}, \text{Re}\rho_{12}, \text{Im}\rho_{12}, \text{Re}\rho_{13}, \text{Im}\rho_{13}, \dots, \rho_{44}]^T.$$

Conversely, a two-qubit density matrix  $\rho$  can be represented as a real vector  $x = (x_1, \dots, x_{16})$  with its elements

given as follows

$$\rho(x) = \begin{bmatrix} x_1 & x_2 + ix_3 & x_4 + ix_5 & x_6 + ix_7 \\ x_2 - ix_3 & x_8 & x_9 + ix_{10} & x_{11} + ix_{12} \\ x_4 - ix_5 & x_9 - ix_{10} & x_{13} & x_{14} + ix_{15} \\ x_6 - ix_7 & x_{11} - ix_{12} & x_{14} - ix_{15} & x_{16} \end{bmatrix}$$

The already mentioned condition number  $\kappa$  depends only on  $A$ , i.e., the system of equations used to estimate the density matrix from the experimental data  $b$ . The reliability of the reconstructed density matrix  $\rho$  corresponding to the vector  $x = A^{-1}b$  for a given set of rotations  $A$  (representing our linear tomographic system) and for the measured data  $b$  depends on the value of  $\kappa$ . To show the operational (or physical) importance of condition numbers more explicitly, let us recall a well known theorem (Theorem 8.4 in Ref. [33]): Consider the system  $Ax = b$  with nonsingular  $A$ . Assume perturbations  $\delta b$  in  $b$ . If perturbations  $\delta x$  are defined implicitly by  $A(x + \delta x) = b + \delta b$ , then it holds [33]:

$$\frac{1}{\kappa(A)} \frac{\|\delta b\|}{\|b\|} \leq \frac{\|\delta x\|}{\|x\|} \leq \kappa(A) \frac{\|\delta b\|}{\|b\|}. \quad (1)$$

Thus, if the condition number  $\kappa(A)$ , for a given norm, is equal (or very close) to one, then small relative changes in the observation vector  $b$  imply equally small relative changes in the reconstructed state  $x$ . Here we calculate  $\kappa(A) \equiv \text{cond}_2(A) = \sigma_{\max}(A)/\sigma_{\min}(A)$  based on the spectral norm  $\|A\|_2$ , which is compatible with Euclidean distance  $\|\cdot\|$  used for other quantities in Eq. (1). The norm is defined by the largest singular value of  $A$ , i.e.,  $\|A\|_2 = \max[\text{svd}(A)] \equiv \sigma_{\max}(A)$ , where the function  $\text{svd}(A)$  returns the singular values of  $A$ . As shown in Ref. [29], the optimal tomography provides  $\kappa(A) = 1$  for 16 local and nonlocal measurements. By contrast to this, the JKMW tomography [4] leads to  $\kappa(A) = \sqrt{60.1}$  for 16 local measurements, the standard separable basis [20, 32] yields  $\kappa(A) = 3$  for 36 local measurements, and mutually-unbiased bases [22, 34] gives  $\kappa(A) = \sqrt{5}$  for 20 local and nonlocal measurements. The tomography based on Pauli matrices gives  $\kappa(A) = \sqrt{2}$  for 16 local measurements. This suggest that the density matrices reconstructed with these different protocols reside inside uncertainty circles of various radii that depend on  $\kappa$ .

*Error analysis.*— From the linearity of the linear inversion problem and Eq. (1) it follows that

$$\frac{1}{\kappa(A)} \frac{\|\delta b\|}{\|b + \delta b\|} \leq \frac{\|\delta x\|}{\|x + \delta x\|} \leq \kappa(A) \frac{\|\delta b\|}{\|b + \delta b\|}. \quad (2)$$

Let us quantify the quality of a tomography protocol with the trace distance  $E \equiv T[\rho(x), \rho(x + \delta x)] = \frac{1}{2} \text{Tr} \sqrt{(\delta \rho)^2}$ , where  $\delta \rho \equiv \rho(\delta x)$ , between the ideal,  $\rho(x)$ , and perturbed,  $\rho(x + \delta x)$ , density matrices. The trace distance is a proper measure of the distance between two density matrices and has a statistical interpretation in terms of the

probability of distinguishing between the two matrices. Moreover, it provides a single number that quantifies the error introduced by the protocol. We can relate  $E$  to  $\|\delta x\|$  by using a standard inequality between the quadratic and arithmetic means of eigenvalues of  $\sqrt{(\delta \rho)^2}$ . The result is

$$2E = \text{Tr} \sqrt{(\delta \rho)^2} \leq \sqrt{d} \text{Tr}[(\delta \rho)^2] \leq \sqrt{2d} \|\delta x\|, \quad (3)$$

where, for a two-qubit density matrix,  $\text{Tr}[(\delta \rho)^2] = 2 \sum_{i=1}^{16} \delta x_i^2 - (\delta x_1^2 + \delta x_5^2 + \delta x_{13}^2 + \delta x_{16}^2)$  and the matrix dimension is  $d = 4$ . By combining inequalities in Eqs. (2) and (3) we arrive at

$$E \leq \sqrt{\frac{d}{2}} \kappa(A) \frac{\|\delta b\| \|x + \delta x\|}{\|b + \delta b\|}, \quad (4)$$

where the random deviations  $\delta b$  can be related to the vector of standard deviations  $\sigma(b)$  associated with the mean values  $b$ . The distribution of random photon counts  $b + \delta b$  is usually described by the Poisson statistics. After performing the measurements  $b + \delta b$  one assumes that  $b + \delta b \approx b = \sigma^2(b)$ , i.e., the measurement outcomes are the most likely (the mean) number of counts. The relative error of such approximation is small if the number of counts is large. In order to compare the robustness of the tomographies, the deviations  $\delta b$  need to be bounded from above. For the Poisson distribution, the probability of a magnitude of a random deviation,  $|\delta b_i| > 2\sqrt{2b_i}$ , is given by its cumulative distribution function (CDF) as  $\text{Pr}(|\delta b_i| > 2\sqrt{2b_i}) = \text{CDF}(x_+) - \text{CDF}(x_-)$ , where  $x_{\pm} = [b_i \pm 2\sqrt{2b_i}]$  and for the Poisson distribution  $\text{CDF}(x < 0) = 0$ . The probability  $\text{Pr}(|\delta b_i| > 2\sqrt{2b_i}) > 0.981$  is very high for all  $b_i$ . For  $b_i > 20$  its value is already  $\text{Pr}(|\delta b_i| > 2\sqrt{2b_i}) > 0.993$ . The same approach applied to the Gaussian distribution provides the widely used  $3\sigma$  rule, which tells us that almost certainly (with probability 0.997)  $|\delta b_i| < 3\sigma(b_i)$ . The statistically justified inequality  $|\delta b_i| < 2\sqrt{2}\sigma(b_i)$  leads to

$$E \leq R \equiv 2\sqrt{d} \kappa(A) \frac{\|\sigma(b)\| \|x + \delta x\|}{\|b + \delta b\|}. \quad (5)$$

We have defined the uncertainty radius of the state estimation  $R$ , which is the maximal distance between the state and its estimate, in terms of only the directly measured quantities. This is an important result as it allows to directly estimate the quality of a given state reconstruction in a very convenient way. As we will demonstrate, it also allows to visually compare the outcomes of various tomographies. This result allows to easily characterize the quality of reconstruction without knowing  $\rho$  a priori. Moreover,  $R$  can be used as a sanity check for the results of maximum likelihood methods, because the proper density matrices should be contained within the uncertainty circle of a radius  $R$ .

However, using the uncertainty radius  $R$ , one can overestimate the value of the disturbance  $E$ . Let us introduce

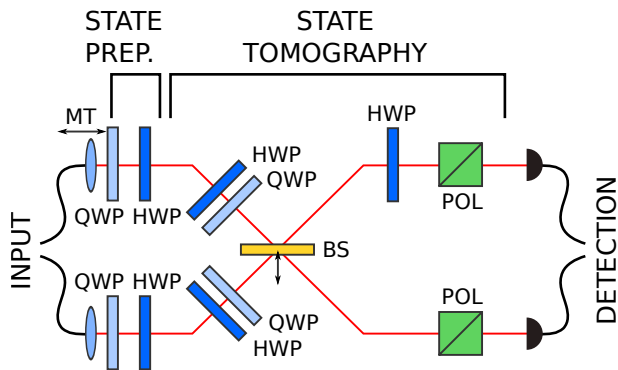


FIG. 1. Experimental setup performing both local and nonlocal polarization projections for the four studied tomographies. Linear-optical components are quarter-wave plate (QWP), half-wave plate (HWP), motorized translation (MT) to stabilize two-photon overlap, horizontally retractable balanced beam splitter (BS), polarizing cube (POL).

$k = \|\delta b\|/\|\sigma(b)\|$ , where  $0 \leq k \leq 2\sqrt{2}$  for the Poissonian statistics. In the most general case we can write

$$\frac{kR}{4\sqrt{d}\kappa^2(A)} \leq E \leq \frac{kR}{2\sqrt{2}}, \quad (6)$$

where the lower bound is derived with help of Eqs. (4) and (5), and the relation between the trace distance and the Hilbert-Schmidt distance  $D_{\text{HS}}(\rho, \rho + \delta\rho) = \sqrt{\text{Tr}[(\delta\rho)^2]} \leq 2E$ . For an arbitrary distribution of the results  $b_i$ , the Chebyshev's inequality implies that the probability of finding the reconstructed state inside of an error circle of the radius  $kR/2\sqrt{2}$  is bounded from below by  $1 - 1/k^2$ . This means that the minimum of 50% of values must lie within the  $\sqrt{2}$  standard deviations of the mean regardless of the distribution, i.e., the value of  $R/2$  bounds from above the median of  $E$  for any distribution. For the Poisson distribution we can find a tighter upper bound on the probability of  $b_i + \delta b_i > b_i + k\sigma(b_i)$  than the one provided by the Chebyshev inequality, i.e.,  $\text{Pr}(X > x) \leq e^{-\mu}(e\mu/x)^x$  (Theorem 5.4 in Ref. [35]), where  $X = b_i + \delta b_i$  is the random variable,  $\mu = b_i$  and  $x = \mu + k\sqrt{\mu}$ .

For characterizing the quality of tomographic protocols we can also introduce the disturbance  $D_B(\rho, \rho + \delta\rho) = 1 - [\text{Tr}\sqrt{\sqrt{\rho}(\rho + \delta\rho)\sqrt{\rho}}]^2 = 1 - F(\rho, \rho + \delta\rho)$ , where  $F$  is the fidelity related to Bures metrics, which fulfils  $D_B(\rho, \rho + \delta\rho) \leq T(\rho, \rho + \delta\rho)$ . Thus,  $D_B \leq E \leq R$ . The disturbance was used in Ref. [22] for comparing the results of two-qubit tomographies. However, in our analysis we apply the trace distance as it provides a more convenient theoretical framework.

*Experimental results.*— The results obtained in the previous section suggest that the error  $E$  of state estimation depends both on  $\kappa(A)$  and the measured quantities  $b_i$ . Therefore, in order to compare the above-mentioned

tomographic protocols we have prepared 17 two-qubit states and performed four tomographic protocols on each of them. These states are two-photon states described in the polarization basis  $\{HH, HV, VH, VV\}$ . This means that, e.g.,  $\rho_{11} = x_1$  is the probability of detecting the two photons in the polarization state  $|HH\rangle$  (both photons are polarized horizontally). We have generated separable and polarization-entangled photon pairs using the process of spontaneous parametric down-conversion occurring in a pair of BBO crystals (the so-called Kwiat *et al.* source [36]). With our source, we have observed about  $2 \cdot 10^3$  two-photon detections per second having 200 mW of pumping power at 355 nm. Generated photons were subsequently brought to the input of our tomography setup (see Fig. 1), where the required states were prepared and subsequently both the local and nonlocal polarizations projections were performed. The preparation of a given state was achieved using pairs of half (HWP) and quarter (QWP) wave plates in the input mode of each photon.

In order to perform local projections on individual photons, we have shifted the beam splitter BS horizontally so that the reflections are no longer coupled to the output ports. Then for each local projection, we have adjusted the HWP and QWP in each photon's path and then subjected the photons to a polarizing cube. Respective two-photon detections were registered for 5 seconds.

The nonlocal projections are achieved by combining the local state transformations using the HWPs and QWPs with the singlet-state projection on a balanced beam splitter BS. For this procedure to work, an additional HWP (set to  $45^\circ$ ) has to be placed in one output mode of the beam splitter before the photons are subjected to the polarizers. Again, the two-photon detections were counted for 5 seconds.

While evidently the beam splitter is superfluous for local projections and the polarizing cubes are unnecessary for the nonlocal projections, we maintain all the components in the setup for all times deliberately since we need to compare the observed detection rates across local and nonlocal measurements. This would be problematic without keeping all the components in the setup since the components introduce different technological losses (e.g. back-reflections, scattering). Further to that, our setup allows to switch between the local and nonlocal projections without much effort.

For each tomography we have gathered the coincidence counts  $b + \delta b$  for the specific projectors (see the Supplement [37]). After performing the measurements we estimated the standard deviations as  $b + \delta b \approx b = \sigma^2(b)$ . This is justified for large values of  $b_i$  as the relative error of estimating  $\sigma(b_i)$  from  $b_i + \delta b_i$  is  $< (2\sqrt{2}/\sqrt{b_i})^{1/2}$ . In our experiment, we observe on average that  $b_i \approx 10^3$  and the smallest values of  $\sigma(b_i)$  do not contribute much to  $\|\sigma(b)\|$ . Thus, in order to correct for possible underestimation of  $\|\sigma(b)\|$ , we rescale this value by a factor of

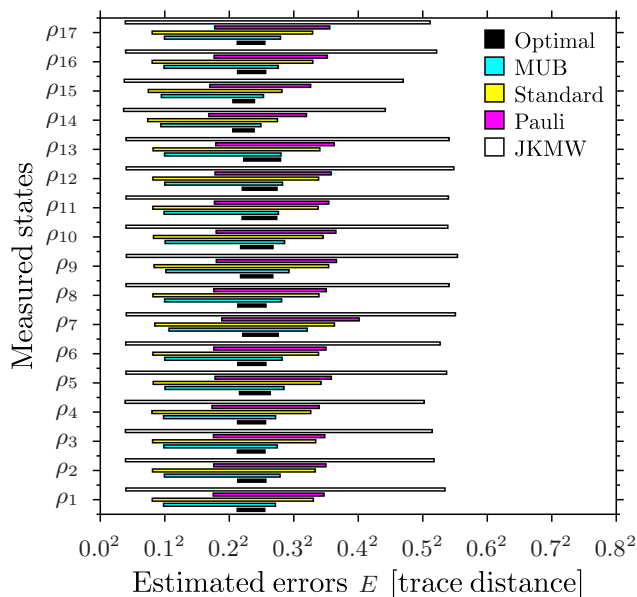


FIG. 2. Experimentally recovered range of possible errors  $E$  for five tomographies (including the optimal, MUB, standard-separable-basis, Pauli operators, and JKMW protocols) for 17 different two-qubit states. The shaded areas correspond to the most probable range of the error  $E$ , given by Eq. (6) for  $k = \sqrt{2}$ . The maximum error  $R$  is twice the upper limit  $r = R/2$  of the plotted error range [see Eq. (5)].

1.3. In most of the tomographies, the observation vector  $b + \delta b$  is measured directly. However, for the optimal tomography [29] there are 12 measurements which correspond to the difference of two coincidence counts, say  $c_i$  and  $c'_i$ . In these cases, the corresponding entries of the observation vector  $b$  are  $b_i = \lfloor (c_i - c'_i)/2 \rfloor$  are described by the Skellam distribution (a generalized Poisson distribution), where  $\sigma^2(b_i) = \lfloor (c_i + c'_i)/2 \rfloor$ . For the Skellam distribution (similarly to the Poisson distribution) the behaviour of its cumulative distribution function implies that the largest disturbance can be limited (with probability  $> 0.993$  for  $c_i, c'_i > 20$ ) by  $\delta b_i \leq \lfloor 2\sqrt{2}\sigma(b_i) \rfloor$ . The results of our analysis are shown in Fig. 2. The figure demonstrates that the error range  $E$  increases with the condition number  $\kappa$  while using the same setup. This suggests that the optimal tomography can truly be the best. A more convincing evidence of this observation is provided by analyzing the relative (trace) distances between the matrices reconstructed by various tomographies and the sizes of their error circles  $r = R/2$ . We know that the unperturbed density matrix must be found in the intersection of the error circles. This intersection is very close to the result of the optimal tomography because it has the smallest error radius. Four selected representative examples of such geometric construction are shown in Fig. 3. Our results for all the reconstructed states can be found in the Supplement [37].

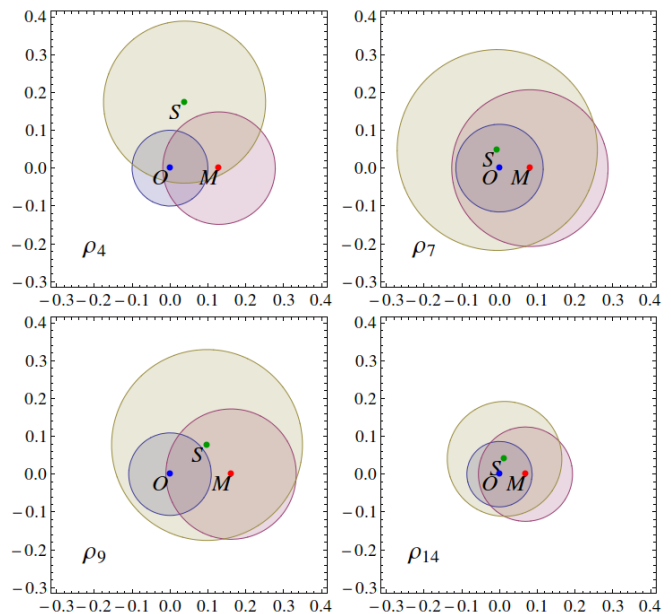


FIG. 3. Relative trace distances between points corresponding to optimal tomography ( $O$ ), standard 36 state tomography ( $S$ ), MUB-based tomography ( $M$ ) representing reconstructed density matrices and their corresponding disks of the maximum errors  $R$  for four selected reconstructed states. All the graphically represented distances scaled in the units of trace distance. The four reconstructed states can be approximated with  $\rho_n = |\psi_n\rangle\langle\psi_n|$ , where  $|\psi_4\rangle = (|DR\rangle - i|AL\rangle)/\sqrt{2}$ ,  $|\psi_7\rangle = |HV\rangle$ ,  $|\psi_9\rangle = (|HV\rangle - |VH\rangle)/\sqrt{2}$ ,  $|\psi_{14}\rangle = |e_{1a}e_{1b}\rangle$ , where  $|e_{1a}\rangle = (-0.6556 + 0.6248i)|H\rangle + 0.4241|V\rangle$  and  $|e_{1b}\rangle = (-0.1415 - 0.7165i)|H\rangle + 0.6831|V\rangle$ , where  $|H\rangle$ ,  $|V\rangle$ ,  $|D\rangle$ ,  $|A\rangle$ ,  $|R\rangle$ , and  $|L\rangle$  stand for the horizontal, vertical, diagonal, anti-diagonal, left-circular, and right circular states, respectively. An ideally reconstructed state lies in the intersection of all the error disks of radius  $R$ . Note that the discs of radius  $R/2$ , associated with the most probable range of errors  $E$  (see Fig. 2), do not necessarily intersect.

*Conclusions.* — We have for the first time implemented the optimal two-qubit tomography and compared it with the other four important tomographic protocols. This method corresponds to measuring one by one all the elements  $\rho_{nm}$  of a density matrix  $\rho$ . This is in contrast to the other protocols, where the off-diagonal elements of  $\rho$  are measured indirectly, i.e., the measured photon numbers correspond to linear combinations of some elements  $\rho_{nm}$ . We have developed a method for estimating the error radii (in units of the trace distance) of circles containing the reconstructed density matrices. We have demonstrated that all the tomographies can be implemented and compared using the same framework. Our results confirm that the optimal tomography provides the most reliable results among all other analyzed protocols. This makes the optimal tomography a method of choice if the quality of the reconstructed density matrix is a priority.

*Acknowledgments.* — K.B. acknowledges the support

by the Polish National Science Centre (Grant No. DEC-2013/11/D/ST2/02638) and by the Foundation for Polish Science (START Programme). K.B. and A.Č. are supported by the project No. LO1305 of the Ministry of Education, Youth and Sports of the Czech Republic. K.L. acknowledges support by the Czech Science Foundation (Grant No.13-31000P). A.M. is supported by the Polish National Science Centre under grants DEC-2011/03/B/ST2/01903 and DEC-2011/02/A/ST2/00305.

---

\* bark@amu.edu.pl

- [1] M. G. A. Paris and J. Řeháček (eds.), *Quantum State Estimation*, Lecture Notes in Physics, Vol. 649 (Springer, Berlin, 2004).
- [2] I. Georgescu and F. Nori, “Quantum technologies: an old new story,” *Phys. World*, p. 16 (May 2012).
- [3] M. A. Nielsen and I. L. Chuang, *Quantum Computation and Quantum Information* (Cambridge University Press, Cambridge, England, 2001).
- [4] D. F. V. James, P. G. Kwiat, W. J. Munro, and A. G. White, “Measurement of qubits,” *Phys. Rev. A* **64**, 052312 (2001).
- [5] J. Řeháček, Z. Hradil, and M. Ježek, “Iterative algorithm for reconstruction of entangled states,” *Phys. Rev. A* **63**, 040303(R) (2001).
- [6] R. Blume-Kohout, “Hedged maximum likelihood quantum state estimation,” *Phys. Rev. Lett.* **105**, 200504 (2010).
- [7] Y. S. Teo, H. Zhu, B. G. Englert, J. Řeháček, and Z. Hradil, “Quantum-state reconstruction by maximizing likelihood and entropy,” *Phys. Rev. Lett.* **107**, 020404 (2011).
- [8] Y. S. Teo, B. Stoklasa, B. G. Englert, J. Řeháček, and Z. Hradil, “Incomplete quantum state estimation: A comprehensive study,” *Phys. Rev. A* **85**, 042317 (2012).
- [9] J. A. Smolin, J. M. Gambetta, and G. Smith, “Efficient method for computing the maximum-likelihood quantum state from measurements with additive Gaussian noise,” *Phys. Rev. Lett.* **108**, 070502 (2012).
- [10] E. Halenková, K. Lemr, A. Černocho, and J. Soubusta, “Experimental simulation of a polarization-dispersion-fluctuating channel with photon pairs,” *Phys. Rev. A* **85**, 063807 (2012).
- [11] E. Halenková, A. Černocho, K. Lemr, J. Soubusta, and S. Drusová, “Experimental implementation of the multifunctional compact two-photon state analyzer,” *Appl. Opt.* **51**, 474 (2012).
- [12] K. Lemr, K. Bartkiewicz, A. Černocho, J. Soubusta, and A. Miranowicz, “Experimental linear-optical implementation of a multifunctional optimal cloner,” *Phys. Rev. A* **85**, 050307(R) (2012).
- [13] K. Bartkiewicz, K. Lemr, A. Černocho, J. Soubusta, and A. Miranowicz, “Experimental eavesdropping based on optimal quantum cloning,” *Phys. Rev. Lett.* **110**, 173601 (2013).
- [14] K. Bartkiewicz, A. Černocho, K. Lemr, J. Soubusta, and M. Stobińska, “Efficient amplification of photonic qubits by optimal quantum cloning” *Phys. Rev. A* **89**, 062322 (2014).
- [15] T. Opatrny, D.-G. Welsch, and W. Vogel, “Least-squares inversion for density-matrix reconstruction,” *Phys. Rev. A* **56**, 1788 (1997).
- [16] R. Blume-Kohout, “Optimal reliable estimation of quantum states,” *New J. Phys.* **12**, 043034 (2010).
- [17] F. Huszár and N. M. T. Houlshby, “Adaptive Bayesian quantum tomography,” *Phys. Rev. A* **85**, 052120 (2012).
- [18] B. Qi, Z. Hou, L. Li, D. Dong, G. Xiang, and G. Guo, “Quantum state tomography via linear regression estimation,” *Sci. Rep.* **3**, 3496 (2013).
- [19] J. B. Altepeter, E. R. Jeffrey, and P. G. Kwiat, “Photonic state tomography,” *Advances in Atomic, Molecular, and Optical Physics* **52**, 105 (2005).
- [20] M. D. de Burgh, N. K. Langford, A. C. Doherty, and A. Gilchrist, “Choice of measurement sets in qubit tomography,” *Phys. Rev. A* **78**, 052122 (2008).
- [21] Yu. I. Bogdanov, G. Brida, M. Genovese, S. P. Kulik, E. V. Moreva, and A. P. Shurupov, “Statistical Estimation of the Efficiency of Quantum State Tomography Protocols,” *Phys. Rev. Lett.* **105**, 010404 (2010).
- [22] R. B. A. Adamson and A. M. Steinberg, “Improving quantum state estimation with mutually unbiased bases,” *Phys. Rev. Lett.* **105**, 030406 (2010).
- [23] L. Sansoni, F. Sciarrino, G. Vallone, P. Mataloni, A. Crespi, R. Ramponi, and R. Osellame, “Polarization Entangled State Measurement on a Chip,” *Phys. Rev. Lett.* **105**, 200503 (2010).
- [24] J. B. Altepeter, N. N. Oza, M. Medić, E. R. Jeffrey, and P. Kumar, “Entangled photon polarimetry,” *Opt. Express* **19**, 26011 (2011).
- [25] G. J. Pryde, J. L. O’Brien, A. G. White, S. D. Bartlett, and T. C. Ralph, “Measuring a Photonic Qubit without Destroying It,” *Phys. Rev. Lett.* **21**, 190402 (2004).
- [26] J. S. Lundeen, B. Sutherland, and A. Patel, “Direct measurement of the quantum wavefunction,” *Nature (London)* **474**, 188 (2011).
- [27] J. S. Lundeen and C. Bamber, “Procedure for Direct Measurement of General Quantum States Using Weak Measurement,” *Phys. Rev. Lett.* **108**, 070402 (2012).
- [28] J. Z. Salvail, M. Agnew, A. S. Johnson, E. Bolduc, J. Leach, and R. W. Boyd, “Full characterization of polarization states of light via direct measurement,” *Nat. Photon.* **7**, 316 (2013).
- [29] A. Miranowicz, K. Bartkiewicz, J. Peřina Jr., M. Koashi, N. Imoto, F. Nori, “Optimal two-qubit tomography based on local and global measurements: Maximal robustness against errors as described by condition numbers,” *Phys. Rev. A* **90**, 062123 (2014).
- [30] Yu. I. Bogdanov, S. P. Kulik, E. V. Moreva, I. V. Tikhonov, and A. K. Gavrichenk, “Optimization of a Quantum Tomography Protocol for Polarization Qubits,” *JETP Letters* **91**, 686 (2010).
- [31] Yu. I. Bogdanov, G. Brida, I. D. Bukeev, M. Genovese, K. S. Kravtsov, S. P. Kulik, E. V. Moreva, A. A. Soloviev, and A. P. Shurupov, “Statistical estimation of the quality of quantum-tomography protocols,” *Phys. Rev. A* **84**, 042108 (2011).
- [32] J. B. Altepeter, E. R. Jeffrey, and P. G. Kwiat, “Phase-compensated ultra-bright source of entangled photons,” *Opt. Express* **13**, 8951 (2005).
- [33] K. E. Atkinson, *An Introduction to Numerical Analysis* (Wiley, New York, 1989).
- [34] S. Bandyopadhyay, P. O. Boykin, V. Roychowdhury, and

- F. Vatan, “A new proof for the existence of mutually unbiased bases,” *Algorithmica* **34**, 512 (2002), arXiv:quant-ph/0103162v3.
- [35] M. Mitzenmacher and E. Upfal, *Probability and Computing: Randomized Algorithms and Probabilistic Analysis* (Cambridge University Press, New York, USA, 2009).
- [36] P. G. Kwiat, E. Waks, A. G. White, I. Appelbaum, and P. H. Eberhard, “Ultrabright source of polarization-entangled photons,” *Phys. Rev. A* **60**, 773 (1999).
- [37] See Supplemental Material for the explicit form of the reconstructed density matrices, coefficient matrices, observation vectors, lists of relevant measurements, and additional figures.

# Priority Choice Experimental Two-qubit Tomography: Measuring One by One All Elements of Density Matrices: Supplementary Materials

Here we show explicitly all the density matrices discussed in the Letter, which are reconstructed with the optimal tomographic protocol and those based on: (i) mutually unbiased bases, (ii) the James-Kwiat-Munro-White projectors, (iii) the tensor products of the Pauli operators, and (iv) the standard separable basis corresponding to all the eigenvectors of the Pauli operators. We also present the coefficient matrices, observation vectors corresponding to coincidence counts, the estimated variances for the observations, and the error radii for each reconstructed matrix. Finally, we compare the reconstructed matrices graphically, where we show the relative trace distances between the reconstructed states and they error radii.

## Reconstructed density matrices

The 17 density matrices are reconstructed by solving linear inversion problem for four tomographies. We have prepared 17 different states of high purity, which approximately correspond to:

$$\begin{aligned}
 |\psi_1\rangle &= (|HH\rangle - |VV\rangle)/\sqrt{2}, & |\psi_2\rangle &= (|HH\rangle + |VV\rangle)/\sqrt{2}, & |\psi_3\rangle &= (|HH\rangle - i|VV\rangle)/\sqrt{2}, \\
 |\psi_4\rangle &= (|DR\rangle - i|AL\rangle)/\sqrt{2}, & |\psi_5\rangle &= (|HV\rangle + i|VH\rangle)/\sqrt{2}, & |\psi_6\rangle &= (|HV\rangle + |VH\rangle)/\sqrt{2}, \\
 & |\psi_7\rangle = |HV\rangle, & |\psi_8\rangle &= (|HH\rangle + i|VV\rangle)/\sqrt{2}, & |\psi_9\rangle &= (|HV\rangle - |VH\rangle)/\sqrt{2}, \\
 |\psi_{10}\rangle &= (|HV\rangle - i|VH\rangle)/\sqrt{2}, & |\psi_{11}\rangle &= (|DL\rangle + i|AR\rangle)/\sqrt{2}, & |\psi_{12}\rangle &= (|DL\rangle - i|AR\rangle)/\sqrt{2}, \\
 & |\psi_{13}\rangle = |e_{1a}e_{1b}\rangle, & |\psi_{14}\rangle &= |e_{2a}e_{2b}\rangle, & |\psi_{15}\rangle &= 0.79|HV\rangle - 0.61|VH\rangle, \\
 |\psi_{16}\rangle &= 0.50|HV\rangle - 0.87|VH\rangle, & |\psi_{17}\rangle &= 0.35|HV\rangle - 0.94|VH\rangle;
 \end{aligned} \tag{7}$$

where  $|e_{1a}\rangle = (-0.6556 + 0.6248i)|H\rangle + 0.4241|V\rangle$ ,  $|e_{1b}\rangle = (-0.1415 - 0.7165i)|H\rangle + 0.6831|V\rangle$ ,  $|e_{2a}\rangle = (-0.9608 + 0.2091i)|H\rangle + 0.1822|V\rangle$ , and  $|e_{2b}\rangle = (0.2613 + 0.7338i)|H\rangle + 0.6271|V\rangle$  are single photon elliptic polarization states. We mark the data relevant to a particular tomography as follows: index  $O$  for the optimal tomography;  $S$  for the standard 36-state tomography;  $J$  for the James-Kwiat-Munro-White (JKMW) protocol;  $M$  for the MUB-based tomography;  $P$  for the Pauli matrices based tomography.

## Standard 36-state tomography

$$\begin{aligned}
 \rho_{S,1} &= \begin{bmatrix} 0.4922 & 0.0020 + 0.0156i & -0.0042 + 0.0354i & -0.4607 - 0.0750i \\ 0.0020 - 0.0156i & 0.0047 & -0.0054 + 0.0228i & 0.0255 - 0.0002i \\ -0.0042 - 0.0354i & -0.0054 - 0.0228i & 0.0136 & 0.0184 + 0.0656i \\ -0.4607 + 0.0750i & 0.0255 + 0.0002i & 0.0184 - 0.0656i & 0.4895 \end{bmatrix} \\
 \rho_{S,2} &= \begin{bmatrix} 0.4870 & 0.0029 - 0.0358i & 0.0237 - 0.0103i & 0.4723 + 0.0515i \\ 0.0029 + 0.0358i & 0.0085 & -0.0000 - 0.0219i & 0.0244 + 0.0413i \\ 0.0237 + 0.0103i & -0.0000 + 0.0219i & 0.0038 & -0.0052 - 0.0378i \\ 0.4723 - 0.0515i & 0.0244 - 0.0413i & -0.0052 + 0.0378i & 0.5007 \end{bmatrix} \\
 \rho_{S,3} &= \begin{bmatrix} 0.5363 & 0.0744 - 0.0611i & 0.0830 - 0.0243i & -0.0027 + 0.4636i \\ 0.0744 + 0.0611i & 0.0206 & 0.0522 - 0.0036i & -0.0513 + 0.0602i \\ 0.0830 + 0.0243i & 0.0522 + 0.0036i & 0.0002 & 0.0005 + 0.0402i \\ -0.0027 - 0.4636i & -0.0513 - 0.0602i & 0.0005 - 0.0402i & 0.4429 \end{bmatrix} \\
 \rho_{S,4} &= \begin{bmatrix} 0.3005 & 0.2633 + 0.0250i & 0.0456 - 0.2223i & -0.0648 + 0.2710i \\ 0.2633 - 0.0250i & 0.2482 & 0.0417 - 0.1841i & -0.0334 + 0.2402i \\ 0.0456 + 0.2223i & 0.0417 + 0.1841i & 0.1270 & -0.2145 - 0.0463i \\ -0.0648 - 0.2710i & -0.0334 - 0.2402i & -0.2145 + 0.0463i & 0.3244 \end{bmatrix}
 \end{aligned}$$

$$\rho_{S,5} = \begin{bmatrix} 0.0135 & -0.0859 + 0.0013i & 0.0334 + 0.0685i & 0.0159 + 0.0018i \\ -0.0859 - 0.0013i & 0.5111 & 0.0397 - 0.4647i & -0.0002 - 0.0441i \\ 0.0334 - 0.0685i & 0.0397 + 0.4647i & 0.4697 & 0.0078 - 0.0236i \\ 0.0159 - 0.0018i & -0.0002 + 0.0441i & 0.0078 + 0.0236i & 0.0056 \end{bmatrix}$$

$$\rho_{S,6} = \begin{bmatrix} 0.0146 & 0.0450 + 0.0866i & 0.0849 + 0.0819i & -0.0046 + 0.0341i \\ 0.0450 - 0.0866i & 0.4606 & 0.4608 - 0.0160i & -0.0222 - 0.0282i \\ 0.0849 - 0.0819i & 0.4608 + 0.0160i & 0.5177 & -0.0526 - 0.0125i \\ -0.0046 - 0.0341i & -0.0222 + 0.0282i & -0.0526 + 0.0125i & 0.0072 \end{bmatrix}$$

$$\rho_{S,7} = \begin{bmatrix} 0.0005 & 0.0578 - 0.0482i & 0.0064 + 0.0028i & -0.0088 - 0.0005i \\ 0.0578 + 0.0482i & 0.9915 & 0.0290 + 0.0678i & -0.0436 - 0.1064i \\ 0.0064 - 0.0028i & 0.0290 - 0.0678i & 0.0049 & -0.0043 - 0.0022i \\ -0.0088 + 0.0005i & -0.0436 + 0.1064i & -0.0043 + 0.0022i & 0.0032 \end{bmatrix}$$

$$\rho_{S,8} = \begin{bmatrix} 0.5609 & -0.0543 + 0.0315i & 0.0357 - 0.0364i & 0.0027 - 0.4704i \\ -0.0543 - 0.0315i & 0.0067 & -0.0470 + 0.0079i & -0.0016 + 0.0511i \\ 0.0357 + 0.0364i & -0.0470 - 0.0079i & -0.0091 & 0.0065 - 0.0126i \\ 0.0027 + 0.4704i & -0.0016 - 0.0511i & 0.0065 + 0.0126i & 0.4416 \end{bmatrix}$$

$$\rho_{S,9} = \begin{bmatrix} -0.0208 & -0.0024 - 0.0670i & -0.0036 + 0.0319i & -0.0224 - 0.0403i \\ -0.0024 + 0.0670i & 0.5767 & -0.4584 - 0.0718i & -0.0076 - 0.0478i \\ -0.0036 - 0.0319i & -0.4584 + 0.0718i & 0.4334 & 0.0134 + 0.0045i \\ -0.0224 + 0.0403i & -0.0076 + 0.0478i & 0.0134 - 0.0045i & 0.0107 \end{bmatrix}$$

$$\rho_{S,10} = \begin{bmatrix} -0.0118 & 0.0243 - 0.0103i & 0.0134 + 0.0063i & -0.0090 - 0.0064i \\ 0.0243 + 0.0103i & 0.5080 & 0.0499 + 0.4684i & -0.0174 - 0.0050i \\ 0.0134 - 0.0063i & 0.0499 - 0.4684i & 0.4801 & 0.0302 + 0.0537i \\ -0.0090 + 0.0064i & -0.0174 + 0.0050i & 0.0302 - 0.0537i & 0.0237 \end{bmatrix}$$

$$\rho_{S,11} = \begin{bmatrix} 0.2826 & 0.2502 + 0.0153i & -0.0157 + 0.2358i & 0.0053 - 0.2593i \\ 0.2502 - 0.0153i & 0.2221 & -0.0295 + 0.2241i & 0.0222 - 0.2349i \\ -0.0157 - 0.2358i & -0.0295 - 0.2241i & 0.2718 & -0.2432 + 0.0003i \\ 0.0053 + 0.2593i & 0.0222 + 0.2349i & -0.2432 - 0.0003i & 0.2235 \end{bmatrix}$$

$$\rho_{S,12} = \begin{bmatrix} 0.2100 & -0.2611 - 0.0385i & -0.0419 - 0.2516i & 0.0345 - 0.2156i \\ -0.2611 + 0.0385i & 0.2815 & 0.0452 + 0.2460i & 0.0115 + 0.2405i \\ -0.0419 + 0.2516i & 0.0452 - 0.2460i & 0.2312 & 0.2259 + 0.0926i \\ 0.0345 + 0.2156i & 0.0115 - 0.2405i & 0.2259 - 0.0926i & 0.2772 \end{bmatrix}$$

$$\rho_{S,13} = \begin{bmatrix} 0.2849 & -0.2477 - 0.0400i & 0.0073 + 0.2296i & 0.0167 + 0.2654i \\ -0.2477 + 0.0400i & 0.2042 & 0.0104 - 0.2183i & -0.0427 - 0.2274i \\ 0.0073 - 0.2296i & 0.0104 + 0.2183i & 0.2687 & 0.2297 - 0.0240i \\ 0.0167 - 0.2654i & -0.0427 + 0.2274i & 0.2297 + 0.0240i & 0.2422 \end{bmatrix}$$

$$\rho_{S,14} = \begin{bmatrix} 0.3786 & -0.0779 - 0.3764i & -0.1289 + 0.1049i & 0.1243 + 0.0775i \\ -0.0779 + 0.3764i & 0.3745 & -0.0776 - 0.1422i & -0.0950 + 0.1000i \\ -0.1289 - 0.1049i & -0.0776 + 0.1422i & 0.1345 & -0.0377 - 0.1163i \\ 0.1243 - 0.0775i & -0.0950 - 0.1000i & -0.0377 + 0.1163i & 0.1124 \end{bmatrix}$$



$$\rho_{S,15} = \begin{bmatrix} 0.5241 & 0.1701 + 0.4098i & -0.0732 + 0.0497i & -0.0613 - 0.0740i \\ 0.1701 - 0.4098i & 0.3733 & 0.0048 + 0.0800i & -0.0776 + 0.0176i \\ -0.0732 - 0.0497i & 0.0048 - 0.0800i & 0.0586 & 0.0165 + 0.0519i \\ -0.0613 + 0.0740i & -0.0776 - 0.0176i & 0.0165 - 0.0519i & 0.0440 \end{bmatrix}$$

$$\rho_{S,16} = \begin{bmatrix} 0.0079 & -0.0088 - 0.1191i & -0.0026 + 0.0469i & -0.0179 - 0.0369i \\ -0.0088 + 0.1191i & 0.6443 & -0.4307 - 0.0597i & -0.0144 - 0.0826i \\ -0.0026 - 0.0469i & -0.4307 + 0.0597i & 0.3254 & 0.0248 + 0.0298i \\ -0.0179 + 0.0369i & -0.0144 + 0.0826i & 0.0248 - 0.0298i & 0.0224 \end{bmatrix}$$

$$\rho_{S,17} = \begin{bmatrix} 0.0071 & -0.0098 - 0.1224i & -0.0079 + 0.0450i & -0.0180 - 0.0331i \\ -0.0098 + 0.1224i & 0.7482 & -0.3769 - 0.0542i & -0.0215 - 0.1008i \\ -0.0079 - 0.0450i & -0.3769 + 0.0542i & 0.2232 & 0.0274 + 0.0197i \\ -0.0180 + 0.0331i & -0.0215 + 0.1008i & 0.0274 - 0.0197i & 0.0215 \end{bmatrix}$$

### JKMW Tomography

$$\rho_{J,1} = \begin{bmatrix} 0.4879 & -0.0241 + 0.0194i & -0.0198 + 0.0473i & -0.4503 - 0.0438i \\ -0.0241 - 0.0194i & 0.0054 & -0.0313 + 0.1193i & 0.0428 - 0.0066i \\ -0.0198 - 0.0473i & -0.0313 - 0.1193i & 0.0225 & -0.0023 + 0.0852i \\ -0.4503 + 0.0438i & 0.0428 + 0.0066i & -0.0023 - 0.0852i & 0.4842 \end{bmatrix}$$

$$\rho_{J,2} = \begin{bmatrix} 0.4748 & 0.0156 - 0.0702i & -0.0009 + 0.0089i & 0.4543 + 0.0190i \\ 0.0156 + 0.0702i & 0.0107 & 0.0457 - 0.1052i & 0.0248 + 0.0104i \\ -0.0009 - 0.0089i & 0.0457 + 0.1052i & 0.0079 & 0.0098 - 0.0398i \\ 0.4543 - 0.0190i & 0.0248 - 0.0104i & 0.0098 + 0.0398i & 0.5065 \end{bmatrix}$$

$$\rho_{J,3} = \begin{bmatrix} 0.5221 & 0.0753 - 0.0707i & 0.0706 - 0.0238i & 0.0314 + 0.4451i \\ 0.0753 + 0.0707i & 0.0213 & 0.0016 - 0.0338i & -0.0532 + 0.0446i \\ 0.0706 + 0.0238i & 0.0016 + 0.0338i & 0.0112 & 0.0008 + 0.0618i \\ 0.0314 - 0.4451i & -0.0532 - 0.0446i & 0.0008 - 0.0618i & 0.4454 \end{bmatrix}$$

$$\rho_{J,4} = \begin{bmatrix} 0.2807 & 0.2535 + 0.0302i & 0.0392 - 0.1853i & -0.0417 + 0.2515i \\ 0.2535 - 0.0302i & 0.2543 & -0.0142 - 0.1473i & -0.0489 + 0.1999i \\ 0.0392 + 0.1853i & -0.0142 + 0.1473i & 0.1256 & -0.2106 - 0.0075i \\ -0.0417 - 0.2515i & -0.0489 - 0.1999i & -0.2106 + 0.0075i & 0.3394 \end{bmatrix}$$

$$\rho_{J,5} = \begin{bmatrix} 0.0260 & -0.0955 + 0.0352i & 0.0370 + 0.0450i & 0.0842 + 0.0143i \\ -0.0955 - 0.0352i & 0.5035 & 0.0139 - 0.4182i & -0.0177 - 0.0134i \\ 0.0370 - 0.0450i & 0.0139 + 0.4182i & 0.4676 & -0.0199 - 0.0215i \\ 0.0842 - 0.0143i & -0.0177 + 0.0134i & -0.0199 + 0.0215i & 0.0029 \end{bmatrix}$$

$$\rho_{J,6} = \begin{bmatrix} 0.0367 & 0.0389 + 0.1059i & 0.0675 + 0.0395i & 0.0312 + 0.0146i \\ 0.0389 - 0.1059i & 0.4500 & 0.4370 - 0.0716i & -0.0533 - 0.0099i \\ 0.0675 - 0.0395i & 0.4370 + 0.0716i & 0.5064 & -0.0482 - 0.0141i \\ 0.0312 - 0.0146i & -0.0533 + 0.0099i & -0.0482 + 0.0141i & 0.0069 \end{bmatrix}$$

$$\rho_{J,7} = \begin{bmatrix} 0.0062 & 0.0456 - 0.0314i & 0.0057 + 0.0030i & 0.0072 - 0.0079i \\ 0.0456 + 0.0314i & 0.9818 & 0.0226 + 0.0910i & -0.0969 - 0.0714i \\ 0.0057 - 0.0030i & 0.0226 - 0.0910i & 0.0032 & -0.0035 + 0.0032i \\ 0.0072 + 0.0079i & -0.0969 + 0.0714i & -0.0035 - 0.0032i & 0.0087 \end{bmatrix}$$

$$\rho_{J,8} = \begin{bmatrix} 0.5550 & -0.0784 + 0.0200i & -0.0058 - 0.0372i & -0.0223 - 0.4409i \\ -0.0784 - 0.0200i & 0.0135 & 0.0219 + 0.0377i & -0.0032 + 0.0374i \\ -0.0058 + 0.0372i & 0.0219 - 0.0377i & 0.0043 & -0.0027 - 0.0162i \\ -0.0223 + 0.4409i & -0.0032 - 0.0374i & -0.0027 + 0.0162i & 0.4271 \end{bmatrix}$$

$$\rho_{J,9} = \begin{bmatrix} 0.0089 & -0.0324 - 0.0301i & -0.0031 - 0.0189i & 0.0009 - 0.0043i \\ -0.0324 + 0.0301i & 0.5684 & -0.4348 + 0.0409i & -0.0166 - 0.0446i \\ -0.0031 + 0.0189i & -0.4348 - 0.0409i & 0.4209 & 0.0002 - 0.0151i \\ 0.0009 + 0.0043i & -0.0166 + 0.0446i & 0.0002 + 0.0151i & 0.0018 \end{bmatrix}$$

$$\rho_{J,10} = \begin{bmatrix} 0.0058 & 0.0400 - 0.0019i & 0.0128 - 0.0240i & -0.0401 - 0.0454i \\ 0.0400 + 0.0019i & 0.5133 & 0.0953 + 0.3781i & -0.0293 + 0.0144i \\ 0.0128 + 0.0240i & 0.0953 - 0.3781i & 0.4753 & 0.0619 + 0.0094i \\ -0.0401 + 0.0454i & -0.0293 - 0.0144i & 0.0619 - 0.0094i & 0.0056 \end{bmatrix}$$

$$\rho_{J,11} = \begin{bmatrix} 0.2918 & 0.2453 - 0.0200i & -0.0285 + 0.1767i & -0.0527 - 0.2169i \\ 0.2453 + 0.0200i & 0.1992 & 0.0202 + 0.2358i & 0.0220 - 0.2014i \\ -0.0285 - 0.1767i & 0.0202 - 0.2358i & 0.2948 & -0.2464 + 0.0008i \\ -0.0527 + 0.2169i & 0.0220 + 0.2014i & -0.2464 - 0.0008i & 0.2142 \end{bmatrix}$$

$$\rho_{J,12} = \begin{bmatrix} 0.1923 & -0.2367 - 0.0390i & -0.0338 - 0.1873i & -0.0453 - 0.2798i \\ -0.2367 + 0.0390i & 0.3002 & 0.0996 + 0.1912i & 0.0039 + 0.2219i \\ -0.0338 + 0.1873i & 0.0996 - 0.1912i & 0.2127 & 0.2404 + 0.0740i \\ -0.0453 + 0.2798i & 0.0039 - 0.2219i & 0.2404 - 0.0740i & 0.2947 \end{bmatrix}$$

$$\rho_{J,13} = \begin{bmatrix} 0.3064 & -0.2350 - 0.0157i & 0.0162 + 0.1740i & 0.0769 + 0.2162i \\ -0.2350 + 0.0157i & 0.1884 & -0.0753 - 0.2582i & -0.0327 - 0.1833i \\ 0.0162 - 0.1740i & -0.0753 + 0.2582i & 0.2840 & 0.2538 - 0.0131i \\ 0.0769 - 0.2162i & -0.0327 + 0.1833i & 0.2538 + 0.0131i & 0.2211 \end{bmatrix}$$

$$\rho_{J,14} = \begin{bmatrix} 0.3803 & -0.0676 - 0.4027i & -0.1333 + 0.1142i & 0.1197 + 0.1053i \\ -0.0676 + 0.4027i & 0.3748 & -0.0745 - 0.1464i & -0.0932 + 0.1079i \\ -0.1333 - 0.1142i & -0.0745 + 0.1464i & 0.1345 & -0.0335 - 0.1211i \\ 0.1197 - 0.1053i & -0.0932 - 0.1079i & -0.0335 + 0.1211i & 0.1104 \end{bmatrix}$$

$$\rho_{J,15} = \begin{bmatrix} 0.5276 & 0.1690 + 0.4181i & -0.0627 + 0.0920i & -0.0903 - 0.0653i \\ 0.1690 - 0.4181i & 0.3819 & 0.0342 + 0.0807i & -0.0764 + 0.0379i \\ -0.0627 - 0.0920i & 0.0342 - 0.0807i & 0.0478 & 0.0032 + 0.0440i \\ -0.0903 + 0.0653i & -0.0764 - 0.0379i & 0.0032 - 0.0440i & 0.0427 \end{bmatrix}$$

$$\rho_{J,16} = \begin{bmatrix} 0.0207 & -0.0045 - 0.1146i & -0.0112 + 0.0073i & -0.0325 - 0.0020i \\ -0.0045 + 0.1146i & 0.6312 & -0.4297 + 0.0089i & 0.0034 - 0.0464i \\ -0.0112 - 0.0073i & -0.4297 - 0.0089i & 0.3450 & 0.0040 + 0.0183i \\ -0.0325 + 0.0020i & 0.0034 + 0.0464i & 0.0040 - 0.0183i & 0.0031 \end{bmatrix}$$

$$\rho_{J,17} = \begin{bmatrix} 0.0202 & -0.0172 - 0.1220i & -0.0095 + 0.0268i & -0.0629 - 0.0175i \\ -0.0172 + 0.1220i & 0.7415 & -0.3322 - 0.0029i & -0.0138 - 0.0503i \\ -0.0095 - 0.0268i & -0.3322 + 0.0029i & 0.2341 & 0.0108 - 0.0009i \\ -0.0629 + 0.0175i & -0.0138 + 0.0503i & 0.0108 + 0.0009i & 0.0042 \end{bmatrix}$$

## MUB-based tomography

$$\rho_{M,1} = \begin{bmatrix} 0.4789 & 0.0857 + 0.0275i & 0.0044 + 0.0534i & -0.4699 - 0.0476i \\ 0.0857 - 0.0275i & 0.0311 & -0.0110 - 0.0029i & 0.0332 - 0.0196i \\ 0.0044 - 0.0534i & -0.0110 + 0.0029i & -0.0015 & 0.0215 + 0.0758i \\ -0.4699 + 0.0476i & 0.0332 + 0.0196i & 0.0215 - 0.0758i & 0.4915 \end{bmatrix}$$

$$\rho_{M,2} = \begin{bmatrix} 0.4888 & -0.0083 - 0.0456i & 0.0198 + 0.0013i & 0.4919 + 0.0541i \\ -0.0083 + 0.0456i & 0.0296 & 0.0027 - 0.0241i & 0.0206 + 0.0291i \\ 0.0198 - 0.0013i & 0.0027 + 0.0241i & -0.0322 & -0.0820 - 0.0477i \\ 0.4919 - 0.0541i & 0.0206 - 0.0291i & -0.0820 + 0.0477i & 0.5138 \end{bmatrix}$$

$$\rho_{M,3} = \begin{bmatrix} 0.5214 & 0.0980 - 0.0452i & 0.0865 - 0.0535i & 0.0541 + 0.4566i \\ 0.0980 + 0.0452i & 0.0573 & -0.0021 + 0.0016i & -0.0472 + 0.0870i \\ 0.0865 + 0.0535i & -0.0021 - 0.0016i & 0.0053 & -0.0563 + 0.0557i \\ 0.0541 - 0.4566i & -0.0472 - 0.0870i & -0.0563 - 0.0557i & 0.4160 \end{bmatrix}$$

$$\rho_{M,4} = \begin{bmatrix} 0.2423 & 0.2560 + 0.0449i & 0.0503 - 0.2014i & 0.0328 + 0.2533i \\ 0.2560 - 0.0449i & 0.3304 & 0.1157 - 0.1609i & -0.0336 + 0.2319i \\ 0.0503 + 0.2014i & 0.1157 + 0.1609i & 0.1676 & -0.1754 - 0.0308i \\ 0.0328 - 0.2533i & -0.0336 - 0.2319i & -0.1754 + 0.0308i & 0.2597 \end{bmatrix}$$

$$\rho_{M,5} = \begin{bmatrix} -0.0004 & -0.0941 + 0.0188i & 0.0384 + 0.0899i & 0.0017 - 0.0313i \\ -0.0941 - 0.0188i & 0.4975 & 0.1830 - 0.4264i & 0.0052 - 0.0638i \\ 0.0384 - 0.0899i & 0.1830 + 0.4264i & 0.5160 & 0.0302 - 0.0058i \\ 0.0017 + 0.0313i & 0.0052 + 0.0638i & 0.0302 + 0.0058i & -0.0131 \end{bmatrix}$$

$$\rho_{M,6} = \begin{bmatrix} 0.0119 & 0.0116 + 0.0964i & 0.0767 + 0.0744i & 0.0106 + 0.0150i \\ 0.0116 - 0.0964i & 0.4477 & 0.4659 + 0.0031i & -0.0301 - 0.0330i \\ 0.0767 - 0.0744i & 0.4659 - 0.0031i & 0.5525 & -0.0780 - 0.0024i \\ 0.0106 - 0.0150i & -0.0301 + 0.0330i & -0.0780 + 0.0024i & -0.0121 \end{bmatrix}$$

$$\rho_{M,7} = \begin{bmatrix} 0.0377 & 0.0294 - 0.0443i & 0.0050 - 0.0081i & -0.0075 + 0.0315i \\ 0.0294 + 0.0443i & 0.9628 & 0.0006 + 0.0373i & -0.0462 - 0.1064i \\ 0.0050 + 0.0081i & 0.0006 - 0.0373i & 0.0047 & 0.0296 + 0.0029i \\ -0.0075 - 0.0315i & -0.0462 + 0.1064i & 0.0296 - 0.0029i & -0.0052 \end{bmatrix}$$

$$\rho_{M,8} = \begin{bmatrix} 0.5549 & -0.0058 + 0.0214i & 0.0324 + 0.0106i & -0.0598 - 0.4494i \\ -0.0058 - 0.0214i & 0.0236 & 0.0055 - 0.0171i & -0.0052 + 0.0074i \\ 0.0324 - 0.0106i & 0.0055 + 0.0171i & -0.0329 & -0.0199 - 0.0231i \\ -0.0598 + 0.4494i & -0.0052 - 0.0074i & -0.0199 + 0.0231i & 0.4544 \end{bmatrix}$$

$$\rho_{M,9} = \begin{bmatrix} -0.0157 & -0.0020 - 0.0764i & -0.0028 + 0.0180i & -0.0136 - 0.0240i \\ -0.0020 + 0.0764i & 0.5405 & -0.4696 - 0.0885i & -0.0067 - 0.0289i \\ -0.0028 - 0.0180i & -0.4696 + 0.0885i & 0.4525 & 0.0798 - 0.0047i \\ -0.0136 + 0.0240i & -0.0067 + 0.0289i & 0.0798 + 0.0047i & 0.0228 \end{bmatrix}$$

$$\rho_{M,10} = \begin{bmatrix} -0.0061 & -0.0415 - 0.0233i & 0.0029 - 0.0435i & -0.0009 - 0.0034i \\ -0.0415 + 0.0233i & 0.4724 & -0.0159 + 0.4682i & -0.0280 + 0.0304i \\ 0.0029 + 0.0435i & -0.0159 - 0.4682i & 0.4984 & 0.0302 + 0.0410i \\ -0.0009 + 0.0034i & -0.0280 - 0.0304i & 0.0302 - 0.0410i & 0.0353 \end{bmatrix}$$

$$\rho_{M,11} = \begin{bmatrix} 0.3090 & 0.2536 - 0.0020i & -0.0236 + 0.2387i & 0.0049 - 0.2545i \\ 0.2536 + 0.0020i & 0.2169 & -0.0266 + 0.2206i & 0.0128 - 0.2344i \\ -0.0236 - 0.2387i & -0.0266 - 0.2206i & 0.2625 & -0.2126 - 0.0164i \\ 0.0049 + 0.2545i & 0.0128 + 0.2344i & -0.2126 + 0.0164i & 0.2116 \end{bmatrix}$$

$$\rho_{M,12} = \begin{bmatrix} 0.2210 & -0.2802 - 0.0510i & -0.0475 - 0.2454i & -0.0166 - 0.2218i \\ -0.2802 + 0.0510i & 0.2512 & 0.0112 + 0.2530i & 0.0076 + 0.2359i \\ -0.0475 + 0.2454i & 0.0112 - 0.2530i & 0.1993 & 0.1977 + 0.0841i \\ -0.0166 + 0.2218i & 0.0076 - 0.2359i & 0.1977 - 0.0841i & 0.3285 \end{bmatrix}$$

$$\rho_{M,13} = \begin{bmatrix} 0.3059 & -0.2612 - 0.0147i & 0.0146 + 0.2246i & 0.0422 + 0.2544i \\ -0.2612 + 0.0147i & 0.1762 & -0.0175 - 0.2085i & -0.0342 - 0.2370i \\ 0.0146 - 0.2246i & -0.0175 + 0.2085i & 0.2792 & 0.1911 + 0.0008i \\ 0.0422 - 0.2544i & -0.0342 + 0.2370i & 0.1911 - 0.0008i & 0.2387 \end{bmatrix}$$

$$\rho_{M,14} = \begin{bmatrix} 0.4095 & -0.0753 - 0.3984i & -0.1351 + 0.1251i & 0.1159 + 0.0932i \\ -0.0753 + 0.3984i & 0.3649 & -0.0998 - 0.1619i & -0.0991 + 0.1004i \\ -0.1351 - 0.1251i & -0.0998 + 0.1619i & 0.1005 & -0.0384 - 0.1226i \\ 0.1159 - 0.0932i & -0.0991 - 0.1004i & -0.0384 + 0.1226i & 0.1251 \end{bmatrix}$$

$$\rho_{M,15} = \begin{bmatrix} 0.5590 & 0.1688 + 0.4115i & -0.0750 + 0.0461i & -0.0342 - 0.0741i \\ 0.1688 - 0.4115i & 0.3472 & 0.0472 + 0.0803i & -0.0795 + 0.0198i \\ -0.0750 - 0.0461i & 0.0472 - 0.0803i & 0.0258 & 0.0397 + 0.0409i \\ -0.0342 + 0.0741i & -0.0795 - 0.0198i & 0.0397 - 0.0409i & 0.0680 \end{bmatrix}$$

$$\rho_{M,16} = \begin{bmatrix} 0.0095 & -0.0057 - 0.1331i & -0.0030 + 0.0330i & -0.0239 - 0.0074i \\ -0.0057 + 0.1331i & 0.6278 & -0.3716 - 0.0931i & -0.0152 - 0.0669i \\ -0.0030 - 0.0330i & -0.3716 + 0.0931i & 0.3255 & 0.0919 + 0.0219i \\ -0.0239 + 0.0074i & -0.0152 + 0.0669i & 0.0919 - 0.0219i & 0.0372 \end{bmatrix}$$

$$\rho_{M,17} = \begin{bmatrix} 0.0219 & -0.0122 - 0.1428i & -0.0034 + 0.0132i & -0.0230 - 0.0034i \\ -0.0122 + 0.1428i & 0.7250 & -0.3510 - 0.0873i & -0.0176 - 0.0751i \\ -0.0034 - 0.0132i & -0.3510 + 0.0873i & 0.2151 & 0.0860 + 0.0050i \\ -0.0230 + 0.0034i & -0.0176 + 0.0751i & 0.0860 - 0.0050i & 0.0379 \end{bmatrix}$$

### Optimal tomography

$$\rho_{O,1} = \begin{bmatrix} 0.4879 & -0.0194 + 0.0278i & 0.0045 + 0.0413i & -0.4760 - 0.0086i \\ -0.0194 - 0.0278i & 0.0054 & -0.0112 - 0.0003i & 0.0336 + 0.0064i \\ 0.0045 - 0.0413i & -0.0112 + 0.0003i & 0.0225 & -0.0033 + 0.0768i \\ -0.4760 + 0.0086i & 0.0336 - 0.0064i & -0.0033 - 0.0768i & 0.4842 \end{bmatrix}$$

$$\rho_{O,2} = \begin{bmatrix} 0.4748 & 0.0191 - 0.0443i & 0.0193 - 0.0130i & 0.4781 + 0.0019i \\ 0.0191 + 0.0443i & 0.0107 & 0.0026 + 0.0001i & 0.0200 + 0.0379i \\ 0.0193 + 0.0130i & 0.0026 - 0.0001i & 0.0079 & 0.0111 - 0.0464i \\ 0.4781 - 0.0019i & 0.0200 - 0.0379i & 0.0111 + 0.0464i & 0.5065 \end{bmatrix}$$

$$\rho_{O,3} = \begin{bmatrix} 0.5221 & 0.0816 - 0.0442i & 0.0847 - 0.0240i & 0.0530 + 0.4532i \\ 0.0816 + 0.0442i & 0.0213 & -0.0020 - 0.0026i & -0.0463 + 0.0584i \\ 0.0847 + 0.0240i & -0.0020 + 0.0026i & 0.0112 & 0.0095 + 0.0545i \\ 0.0530 - 0.4532i & -0.0463 - 0.0584i & 0.0095 - 0.0545i & 0.4454 \end{bmatrix}$$

$$\rho_{O,4} = \begin{bmatrix} 0.2807 & 0.2569 + 0.0406i & 0.0456 - 0.2118i & 0.0297 + 0.2155i \\ 0.2569 - 0.0406i & 0.2543 & 0.1047 - 0.1856i & -0.0304 + 0.2331i \\ 0.0456 + 0.2118i & 0.1047 + 0.1856i & 0.1256 & -0.2027 - 0.0279i \\ 0.0297 - 0.2155i & -0.0304 - 0.2331i & -0.2027 + 0.0279i & 0.3394 \end{bmatrix}$$

$$\rho_{O,5} = \begin{bmatrix} 0.0260 & -0.0969 + 0.0186i & 0.0380 + 0.0730i & 0.0017 - 0.0078i \\ -0.0969 - 0.0186i & 0.5035 & 0.1813 - 0.4222i & 0.0051 - 0.0374i \\ 0.0380 - 0.0730i & 0.1813 + 0.4222i & 0.4676 & -0.0051 - 0.0057i \\ 0.0017 + 0.0078i & 0.0051 + 0.0374i & -0.0051 + 0.0057i & 0.0029 \end{bmatrix}$$

$$\rho_{O,6} = \begin{bmatrix} 0.0367 & 0.0502 + 0.0923i & 0.0734 + 0.0820i & 0.0102 - 0.0178i \\ 0.0502 - 0.0923i & 0.4500 & 0.4460 - 0.0748i & -0.0288 - 0.0230i \\ 0.0734 - 0.0820i & 0.4460 + 0.0748i & 0.5064 & -0.0430 - 0.0023i \\ 0.0102 + 0.0178i & -0.0288 + 0.0230i & -0.0430 + 0.0023i & 0.0069 \end{bmatrix}$$

$$\rho_{O,7} = \begin{bmatrix} 0.0062 & 0.0557 - 0.0422i & 0.0047 + 0.0036i & -0.0072 + 0.0029i \\ 0.0557 + 0.0422i & 0.9818 & 0.0006 + 0.0380i & -0.0441 - 0.1031i \\ 0.0047 - 0.0036i & 0.0006 - 0.0380i & 0.0032 & -0.0049 + 0.0027i \\ -0.0072 - 0.0029i & -0.0441 + 0.1031i & -0.0049 - 0.0027i & 0.0087 \end{bmatrix}$$

$$\rho_{O,8} = \begin{bmatrix} 0.5550 & -0.0622 + 0.0204i & 0.0308 - 0.0306i & -0.0569 - 0.4699i \\ -0.0622 - 0.0204i & 0.0135 & 0.0053 - 0.0015i & -0.0050 + 0.0533i \\ 0.0308 + 0.0306i & 0.0053 + 0.0015i & 0.0043 & -0.0039 - 0.0220i \\ -0.0569 + 0.4699i & -0.0050 - 0.0533i & -0.0039 + 0.0220i & 0.4271 \end{bmatrix}$$

$$\rho_{O,9} = \begin{bmatrix} 0.0089 & -0.0219 - 0.0731i & -0.0027 + 0.0214i & -0.0130 + 0.0040i \\ -0.0219 + 0.0731i & 0.5684 & -0.4492 + 0.0011i & -0.0065 - 0.0551i \\ -0.0027 - 0.0214i & -0.4492 - 0.0011i & 0.4209 & -0.0068 - 0.0044i \\ -0.0130 - 0.0040i & -0.0065 + 0.0551i & -0.0068 + 0.0044i & 0.0018 \end{bmatrix}$$

$$\rho_{O,10} = \begin{bmatrix} 0.0058 & 0.0406 - 0.0232i & 0.0029 + 0.0025i & -0.0009 + 0.0092i \\ 0.0406 + 0.0232i & 0.5133 & -0.0158 + 0.4665i & -0.0279 - 0.0088i \\ 0.0029 - 0.0025i & -0.0158 - 0.4665i & 0.4753 & 0.0465 + 0.0408i \\ -0.0009 - 0.0092i & -0.0279 + 0.0088i & 0.0465 - 0.0408i & 0.0056 \end{bmatrix}$$

$$\rho_{O,11} = \begin{bmatrix} 0.2918 & 0.2395 - 0.0021i & -0.0242 + 0.2258i & 0.0050 - 0.2663i \\ 0.2395 + 0.0021i & 0.1992 & -0.0274 + 0.2259i & 0.0132 - 0.2382i \\ -0.0242 - 0.2258i & -0.0274 - 0.2259i & 0.2948 & -0.2469 - 0.0169i \\ 0.0050 + 0.2663i & 0.0132 + 0.2382i & -0.2469 + 0.0169i & 0.2142 \end{bmatrix}$$

$$\rho_{O,12} = \begin{bmatrix} 0.1923 & -0.2541 - 0.0502i & -0.0467 - 0.2470i & -0.0163 - 0.2401i \\ -0.2541 + 0.0502i & 0.3002 & 0.0111 + 0.2257i & 0.0075 + 0.2518i \\ -0.0467 + 0.2470i & 0.0111 - 0.2257i & 0.2127 & 0.2396 + 0.0827i \\ -0.0163 + 0.2401i & 0.0075 - 0.2518i & 0.2396 - 0.0827i & 0.2947 \end{bmatrix}$$

$$\rho_{O,13} = \begin{bmatrix} 0.3064 & -0.2359 - 0.0153i & 0.0152 + 0.2270i & 0.0439 + 0.2918i \\ -0.2359 + 0.0153i & 0.1884 & -0.0182 - 0.1992i & -0.0356 - 0.2367i \\ 0.0152 - 0.2270i & -0.0182 + 0.1992i & 0.2840 & 0.2487 + 0.0009i \\ 0.0439 - 0.2918i & -0.0356 + 0.2367i & 0.2487 - 0.0009i & 0.2211 \end{bmatrix}$$

$$\rho_{O,14} = \begin{bmatrix} 0.3803 & -0.0814 - 0.3887i & -0.1318 + 0.1051i & 0.1131 + 0.0665i \\ -0.0814 + 0.3887i & 0.3748 & -0.0973 - 0.1265i & -0.0967 + 0.1000i \\ -0.1318 - 0.1051i & -0.0973 + 0.1265i & 0.1345 & -0.0398 - 0.1196i \\ 0.1131 - 0.0665i & -0.0967 - 0.1000i & -0.0398 + 0.1196i & 0.1104 \end{bmatrix}$$

$$\rho_{O,15} = \begin{bmatrix} 0.5276 & 0.1680 + 0.4105i & -0.0748 + 0.0527i & -0.0341 - 0.0538i \\ 0.1680 - 0.4105i & 0.3819 & 0.0471 + 0.0874i & -0.0793 + 0.0196i \\ -0.0748 - 0.0527i & 0.0471 - 0.0874i & 0.0478 & 0.0094 + 0.0408i \\ -0.0341 + 0.0538i & -0.0793 - 0.0196i & 0.0094 - 0.0408i & 0.0427 \end{bmatrix}$$

$$\rho_{O,16} = \begin{bmatrix} 0.0207 & -0.0261 - 0.1296i & -0.0029 + 0.0401i & -0.0233 - 0.0012i \\ -0.0261 + 0.1296i & 0.6312 & -0.3619 - 0.0096i & -0.0148 - 0.0912i \\ -0.0029 - 0.0401i & -0.3619 + 0.0096i & 0.3450 & 0.0080 + 0.0213i \\ -0.0233 + 0.0012i & -0.0148 + 0.0912i & 0.0080 - 0.0213i & 0.0031 \end{bmatrix}$$

$$\rho_{O,17} = \begin{bmatrix} 0.0202 & -0.0269 - 0.1385i & -0.0033 + 0.0486i & -0.0223 + 0.0155i \\ -0.0269 + 0.1385i & 0.7415 & -0.3405 + 0.0102i & -0.0171 - 0.0985i \\ -0.0033 - 0.0486i & -0.3405 - 0.0102i & 0.2341 & 0.0106 + 0.0049i \\ -0.0223 - 0.0155i & -0.0171 + 0.0985i & 0.0106 - 0.0049i & 0.0042 \end{bmatrix}$$

### Pauli matrices based tomography

$$\rho_{P,1} = \begin{bmatrix} 0.4879 & -0.0194 + 0.0278i & 0.0045 + 0.0413i & -0.4516 - 0.0735i \\ -0.0194 - 0.0278i & 0.0054 & -0.0053 + 0.0223i & 0.0336 + 0.0064i \\ 0.0045 - 0.0413i & -0.0053 - 0.0223i & 0.0225 & -0.0033 + 0.0768i \\ -0.4516 + 0.0735i & 0.0336 - 0.0064i & -0.0033 - 0.0768i & 0.4842 \end{bmatrix}$$

$$\rho_{P,2} = \begin{bmatrix} 0.4748 & 0.0191 - 0.0443i & 0.0193 - 0.0130i & 0.4662 + 0.0508i \\ 0.0191 + 0.0443i & 0.0107 & -0.0000 - 0.0216i & 0.0200 + 0.0379i \\ 0.0193 + 0.0130i & -0.0000 + 0.0216i & 0.0079 & 0.0111 - 0.0464i \\ 0.4662 - 0.0508i & 0.0200 - 0.0379i & 0.0111 + 0.0464i & 0.5065 \end{bmatrix}$$

$$\rho_{P,3} = \begin{bmatrix} 0.5221 & 0.0816 - 0.0442i & 0.0847 - 0.0240i & -0.0026 + 0.4523i \\ 0.0816 + 0.0442i & 0.0213 & 0.0509 - 0.0035i & -0.0463 + 0.0584i \\ 0.0847 + 0.0240i & 0.0509 + 0.0035i & 0.0112 & 0.0095 + 0.0545i \\ -0.0026 - 0.4523i & -0.0463 - 0.0584i & 0.0095 - 0.0545i & 0.4454 \end{bmatrix}$$

$$\rho_{P,4} = \begin{bmatrix} 0.2807 & 0.2569 + 0.0406i & 0.0456 - 0.2118i & -0.0623 + 0.2607i \\ 0.2569 - 0.0406i & 0.2543 & 0.0401 - 0.1770i & -0.0304 + 0.2331i \\ 0.0456 + 0.2118i & 0.0401 + 0.1770i & 0.1256 & -0.2027 - 0.0279i \\ -0.0623 - 0.2607i & -0.0304 - 0.2331i & -0.2027 + 0.0279i & 0.3394 \end{bmatrix}$$

$$\rho_{P,5} = \begin{bmatrix} 0.0260 & -0.0969 + 0.0186i & 0.0380 + 0.0730i & 0.0156 + 0.0018i \\ -0.0969 - 0.0186i & 0.5035 & 0.0389 - 0.4553i & 0.0051 - 0.0374i \\ 0.0380 - 0.0730i & 0.0389 + 0.4553i & 0.4676 & -0.0051 - 0.0057i \\ 0.0156 - 0.0018i & 0.0051 + 0.0374i & -0.0051 + 0.0057i & 0.0029 \end{bmatrix}$$

$$\rho_{P,6} = \begin{bmatrix} 0.0367 & 0.0502 + 0.0923i & 0.0734 + 0.0820i & -0.0044 + 0.0326i \\ 0.0502 - 0.0923i & 0.4500 & 0.4397 - 0.0152i & -0.0288 - 0.0230i \\ 0.0734 - 0.0820i & 0.4397 + 0.0152i & 0.5064 & -0.0430 - 0.0023i \\ -0.0044 - 0.0326i & -0.0288 + 0.0230i & -0.0430 + 0.0023i & 0.0069 \end{bmatrix}$$

$$\rho_{P,7} = \begin{bmatrix} 0.0062 & 0.0557 - 0.0422i & 0.0047 + 0.0036i & -0.0086 - 0.0005i \\ 0.0557 + 0.0422i & 0.9818 & 0.0283 + 0.0662i & -0.0441 - 0.1031i \\ 0.0047 - 0.0036i & 0.0283 - 0.0662i & 0.0032 & -0.0049 + 0.0027i \\ -0.0086 + 0.0005i & -0.0441 + 0.1031i & -0.0049 - 0.0027i & 0.0087 \end{bmatrix}$$

$$\rho_{P,8} = \begin{bmatrix} 0.5550 & -0.0622 + 0.0204i & 0.0308 - 0.0306i & 0.0026 - 0.4514i \\ -0.0622 - 0.0204i & 0.0135 & -0.0451 + 0.0076i & -0.0050 + 0.0533i \\ 0.0308 + 0.0306i & -0.0451 - 0.0076i & 0.0043 & -0.0039 - 0.0220i \\ 0.0026 + 0.4514i & -0.0050 - 0.0533i & -0.0039 + 0.0220i & 0.4271 \end{bmatrix}$$

$$\rho_{P,9} = \begin{bmatrix} 0.0089 & -0.0219 - 0.0731i & -0.0027 + 0.0214i & -0.0215 - 0.0387i \\ -0.0219 + 0.0731i & 0.5684 & -0.4398 - 0.0689i & -0.0065 - 0.0551i \\ -0.0027 - 0.0214i & -0.4398 + 0.0689i & 0.4209 & -0.0068 - 0.0044i \\ -0.0215 + 0.0387i & -0.0065 + 0.0551i & -0.0068 + 0.0044i & 0.0018 \end{bmatrix}$$

$$\rho_{P,10} = \begin{bmatrix} 0.0058 & 0.0406 - 0.0232i & 0.0029 + 0.0025i & -0.0090 - 0.0064i \\ 0.0406 + 0.0232i & 0.5133 & 0.0500 + 0.4689i & -0.0279 - 0.0088i \\ 0.0029 - 0.0025i & 0.0500 - 0.4689i & 0.4753 & 0.0465 + 0.0408i \\ -0.0090 + 0.0064i & -0.0279 + 0.0088i & 0.0465 - 0.0408i & 0.0056 \end{bmatrix}$$

$$\rho_{P,11} = \begin{bmatrix} 0.2918 & 0.2395 - 0.0021i & -0.0242 + 0.2258i & 0.0052 - 0.2556i \\ 0.2395 + 0.0021i & 0.1992 & -0.0291 + 0.2209i & 0.0132 - 0.2382i \\ -0.0242 - 0.2258i & -0.0291 - 0.2209i & 0.2948 & -0.2469 - 0.0169i \\ 0.0052 + 0.2556i & 0.0132 + 0.2382i & -0.2469 + 0.0169i & 0.2142 \end{bmatrix}$$

$$\rho_{P,12} = \begin{bmatrix} 0.1923 & -0.2541 - 0.0502i & -0.0467 - 0.2470i & 0.0350 - 0.2186i \\ -0.2541 + 0.0502i & 0.3002 & 0.0458 + 0.2493i & 0.0075 + 0.2518i \\ -0.0467 + 0.2470i & 0.0458 - 0.2493i & 0.2127 & 0.2396 + 0.0827i \\ 0.0350 + 0.2186i & 0.0075 - 0.2518i & 0.2396 - 0.0827i & 0.2947 \end{bmatrix}$$

$$\rho_{P,13} = \begin{bmatrix} 0.3064 & -0.2359 - 0.0153i & 0.0152 + 0.2270i & 0.0170 + 0.2694i \\ -0.2359 + 0.0153i & 0.1884 & 0.0105 - 0.2216i & -0.0356 - 0.2367i \\ 0.0152 - 0.2270i & 0.0105 + 0.2216i & 0.2840 & 0.2487 + 0.0009i \\ 0.0170 - 0.2694i & -0.0356 + 0.2367i & 0.2487 - 0.0009i & 0.2211 \end{bmatrix}$$

$$\rho_{P,14} = \begin{bmatrix} 0.3803 & -0.0814 - 0.3887i & -0.1318 + 0.1051i & 0.1286 + 0.0801i \\ -0.0814 + 0.3887i & 0.3748 & -0.0803 - 0.1471i & -0.0967 + 0.1000i \\ -0.1318 - 0.1051i & -0.0803 + 0.1471i & 0.1345 & -0.0398 + 0.1196i \\ 0.1286 - 0.0801i & -0.0967 - 0.1000i & -0.0398 + 0.1196i & 0.1104 \end{bmatrix}$$

$$\rho_{P,15} = \begin{bmatrix} 0.5276 & 0.1680 + 0.4105i & -0.0748 + 0.0527i & -0.0633 - 0.0764i \\ 0.1680 - 0.4105i & 0.3819 & 0.0050 + 0.0826i & -0.0793 + 0.0196i \\ -0.0748 - 0.0527i & 0.0050 - 0.0826i & 0.0478 & 0.0094 + 0.0408i \\ -0.0633 + 0.0764i & -0.0793 - 0.0196i & 0.0094 - 0.0408i & 0.0427 \end{bmatrix}$$

$$\rho_{P,16} = \begin{bmatrix} 0.0207 & -0.0261 - 0.1296i & -0.0029 + 0.0401i & -0.0181 - 0.0374i \\ -0.0261 + 0.1296i & 0.6312 & -0.4367 - 0.0605i & -0.0148 - 0.0912i \\ -0.0029 - 0.0401i & -0.4367 + 0.0605i & 0.3450 & 0.0080 + 0.0213i \\ -0.0181 + 0.0374i & -0.0148 + 0.0912i & 0.0080 - 0.0213i & 0.0031 \end{bmatrix}$$

$$\rho_{P,17} = \begin{bmatrix} 0.0202 & -0.0269 - 0.1385i & -0.0033 + 0.0486i & -0.0181 - 0.0334i \\ -0.0269 + 0.1385i & 0.7415 & -0.3803 - 0.0547i & -0.0171 - 0.0985i \\ -0.0033 - 0.0486i & -0.3803 + 0.0547i & 0.2341 & 0.0106 + 0.0049i \\ -0.0181 + 0.0334i & -0.0171 + 0.0985i & 0.0106 - 0.0049i & 0.0042 \end{bmatrix}$$

### Coefficient matrices

All the analyzed tomographies are based on solving the linear-system problem

$$Ax = b,$$

where  $A$  is the *coefficient matrix*,  $b$  is the *observation vector*, and  $x = \text{vec}(\rho)$  is a real vector describing the unknown state  $\rho$ , i.e.,

$$x = \text{vec}(\rho) = [\rho_{11}, \text{Re}\rho_{12}, \text{Im}\rho_{12}, \text{Re}\rho_{13}, \text{Im}\rho_{13}, \dots, \rho_{44}]^T.$$

Thus, a two-qubit density matrix  $\rho$  is represented as a real vector  $x = (x_1, \dots, x_{16})$  with its elements given as follows

$$\rho(x) = \begin{bmatrix} x_1 & x_2 + ix_3 & x_4 + ix_5 & x_6 + ix_7 \\ x_2 - ix_3 & x_8 & x_9 + ix_{10} & x_{11} + ix_{12} \\ x_4 - ix_5 & x_9 - ix_{10} & x_{13} & x_{14} + ix_{15} \\ x_6 - ix_7 & x_{11} - ix_{12} & x_{14} - ix_{15} & x_{16} \end{bmatrix}.$$

The coefficient matrices depend on the choice of the equations used for reconstructing a given density matrix. Below we list the transposed (for typographic reasons) coefficient matrices for the four analyzed tomographic protocols:

$$A_P^T = \begin{bmatrix} 0 & 0 & 0 & 0 & 0 & 2 & 0 & 0 & 2 & 0 & 0 & 0 & 0 & 0 & 0 \\ 0 & 0 & 0 & 0 & 0 & 0 & -2 & 0 & 0 & 2 & 0 & 0 & 0 & 0 & 0 \\ 0 & 0 & 0 & 2 & 0 & 0 & 0 & 0 & 0 & 0 & -2 & 0 & 0 & 0 & 0 \\ 0 & 0 & 0 & 2 & 0 & 0 & 0 & 0 & 0 & 0 & 2 & 0 & 0 & 0 & 0 \\ 0 & 0 & 0 & 0 & 0 & 0 & -2 & 0 & 0 & -2 & 0 & 0 & 0 & 0 & 0 \\ 0 & 0 & 0 & 0 & 0 & -2 & 0 & 0 & 2 & 0 & 0 & 0 & 0 & 0 & 0 \\ 0 & 0 & 0 & 0 & -2 & 0 & 0 & 0 & 0 & 0 & 0 & 2 & 0 & 0 & 0 \\ 0 & 0 & 0 & 0 & -2 & 0 & 0 & 0 & 0 & 0 & 0 & -2 & 0 & 0 & 0 \\ 0 & 2 & 0 & 0 & 0 & 0 & 0 & 0 & 0 & 0 & 0 & 0 & -2 & 0 & 0 \\ 0 & 0 & -2 & 0 & 0 & 0 & 0 & 0 & 0 & 0 & 0 & 0 & 0 & 2 & 0 \\ 1 & 0 & 0 & 0 & 0 & 0 & 0 & -1 & 0 & 0 & 0 & 0 & -1 & 0 & 0 \\ 1 & 0 & 0 & 0 & 0 & 0 & 0 & 1 & 0 & 0 & 0 & 0 & -1 & 0 & 0 \\ 0 & 2 & 0 & 0 & 0 & 0 & 0 & 0 & 0 & 0 & 0 & 0 & 2 & 0 & 0 \\ 0 & 0 & -2 & 0 & 0 & 0 & 0 & 0 & 0 & 0 & 0 & 0 & 0 & -2 & 0 \\ 1 & 0 & 0 & 0 & 0 & 0 & -1 & 0 & 0 & 0 & 0 & 1 & 0 & 0 & -1 \\ 1 & 0 & 0 & 0 & 0 & 0 & 1 & 0 & 0 & 0 & 0 & 1 & 0 & 0 & 1 \end{bmatrix}$$





$$A_M^T = \frac{1}{4} \begin{bmatrix} 2 & 0 & 0 & 4 & 0 & 0 & 0 & 0 & 0 & 0 & 0 & 0 & 2 & 0 & 0 & 0 \\ 0 & 0 & 0 & 0 & 0 & 0 & 0 & 2 & 0 & 0 & 4 & 0 & 0 & 0 & 0 & 2 \\ 2 & 0 & 0 & -4 & 0 & 0 & 0 & 0 & 0 & 0 & 0 & 0 & 2 & 0 & 0 & 0 \\ 0 & 0 & 0 & 0 & 0 & 0 & 0 & 2 & 0 & 0 & -4 & 0 & 0 & 0 & 0 & 2 \\ 1 & 2 & 0 & 0 & -2 & 0 & -2 & 1 & 0 & -2 & 0 & -2 & 1 & 2 & 0 & 1 \\ 1 & -2 & 0 & 0 & -2 & 0 & 2 & 1 & 0 & 2 & 0 & -2 & 1 & -2 & 0 & 1 \\ 1 & 2 & 0 & 0 & 2 & 0 & 2 & 1 & 0 & 2 & 0 & 2 & 1 & 2 & 0 & 1 \\ 1 & -2 & 0 & 0 & 2 & 0 & -2 & 1 & 0 & -2 & 0 & 2 & 1 & -2 & 0 & 1 \\ 0 & 0 & 0 & 0 & 0 & 0 & 0 & 0 & 0 & 0 & 0 & 0 & 2 & 0 & 4 & 2 \\ 0 & 0 & 0 & 0 & 0 & 0 & 0 & 0 & 0 & 0 & 0 & 0 & 2 & 0 & -4 & 2 \\ 2 & 0 & 4 & 0 & 0 & 0 & 0 & 2 & 0 & 0 & 0 & 0 & 0 & 0 & 0 & 0 \\ 2 & 0 & -4 & 0 & 0 & 0 & 0 & 2 & 0 & 0 & 0 & 0 & 0 & 0 & 0 & 0 \\ 2 & 0 & 0 & 0 & 0 & 4 & 0 & 0 & 0 & 0 & 0 & 0 & 0 & 0 & 0 & 2 \\ 2 & 0 & 0 & 0 & 0 & -4 & 0 & 0 & 0 & 0 & 0 & 0 & 0 & 0 & 0 & 2 \\ 0 & 0 & 0 & 0 & 0 & 0 & 0 & 2 & 4 & 0 & 0 & 0 & 2 & 0 & 0 & 0 \\ 0 & 0 & 0 & 0 & 0 & 0 & 0 & 2 & -4 & 0 & 0 & 0 & 2 & 0 & 0 & 0 \\ 1 & 2 & 0 & 0 & 2 & 0 & -2 & 1 & 0 & 2 & 0 & -2 & 1 & -2 & 0 & 1 \\ 1 & -2 & 0 & 0 & -2 & 0 & -2 & 1 & 0 & 2 & 0 & 2 & 1 & 2 & 0 & 1 \\ 1 & -2 & 0 & 0 & 2 & 0 & 2 & 1 & 0 & -2 & 0 & -2 & 1 & 2 & 0 & 1 \\ 1 & 2 & 0 & 0 & -2 & 0 & 2 & 1 & 0 & -2 & 0 & 2 & 1 & -2 & 0 & 1 \end{bmatrix}$$

$$A_O^T = \begin{bmatrix} 1 & 0 & 0 & 0 & 0 & 0 & 0 & 0 & 0 & 0 & 0 & 0 & 0 & 0 & 0 & 0 \\ 0 & 0 & 0 & 0 & 0 & 0 & 1 & 0 & 0 & 0 & 0 & 0 & 0 & 0 & 0 & 0 \\ 0 & 0 & 0 & 0 & 0 & 0 & 0 & 0 & 0 & 0 & 0 & 0 & 1 & 0 & 0 & 0 \\ 0 & 0 & 0 & 0 & 0 & 0 & 0 & 0 & 0 & 0 & 0 & 0 & 0 & 0 & 0 & 1 \\ 0 & 1 & 0 & 0 & 0 & 0 & 0 & 0 & 0 & 0 & 0 & 0 & 0 & 0 & 0 & 0 \\ 0 & 0 & -1 & 0 & 0 & 0 & 0 & 0 & 0 & 0 & 0 & 0 & 0 & 0 & 0 & 0 \\ 0 & 0 & 0 & 1 & 0 & 0 & 0 & 0 & 0 & 0 & 0 & 0 & 0 & 0 & 0 & 0 \\ 0 & 0 & 0 & 0 & -1 & 0 & 0 & 0 & 0 & 0 & 0 & 0 & 0 & 0 & 0 & 0 \\ 0 & 0 & 0 & 0 & 0 & 0 & 0 & 0 & 0 & 0 & 0 & 0 & 1 & 0 & 0 & 0 \\ 0 & 0 & 0 & 0 & 0 & 0 & 0 & 0 & 0 & 0 & 0 & 0 & 0 & 0 & -1 & 0 \\ 0 & 0 & 0 & 0 & 0 & 0 & 0 & 0 & 0 & 1 & 0 & 0 & 0 & 0 & 0 & 0 \\ 0 & 0 & 0 & 0 & 0 & 0 & 0 & 0 & 0 & 0 & -1 & 0 & 0 & 0 & 0 & 0 \\ 0 & 0 & 0 & 0 & 0 & 0 & 0 & 1 & 0 & 0 & 0 & 0 & 0 & 0 & 0 & 0 \\ 0 & 0 & 0 & 0 & 0 & 0 & 0 & 0 & -1 & 0 & 0 & 0 & 0 & 0 & 0 & 0 \\ 0 & 0 & 0 & 0 & 0 & 1 & 0 & 0 & 0 & 0 & 0 & 0 & 0 & 0 & 0 & 0 \\ 0 & 0 & 0 & 0 & 0 & 0 & -1 & 0 & 0 & 0 & 0 & 0 & 0 & 0 & 0 & 0 \end{bmatrix}$$

### Observation vectors

The observation vectors correspond to photon coincidence counts. In reality we measure disturbed quantities  $\bar{b} \equiv b + \delta b$  instead of  $b$ . The observation vectors are column vectors. For convenience we arrange them in arrays, where each column corresponds to one of the 17 reconstructed states.

$$\bar{b} = \begin{bmatrix} b_1 \\ b_2 \\ \vdots \\ b_N \end{bmatrix} \begin{bmatrix} \rho_1 & \rho_2 & \dots & \rho_{17} \\ \bar{b}_{1,1} & \bar{b}_{1,2} & \dots & \bar{b}_{1,17} \\ \bar{b}_{2,1} & \bar{b}_{2,2} & \dots & \bar{b}_{2,17} \\ \vdots & \vdots & \ddots & \vdots \\ \bar{b}_{N,1} & \bar{b}_{N,2} & \dots & \bar{b}_{N,17} \end{bmatrix}$$

Note that the values of  $b$  listed below are not normalized and cannot be interpreted as probabilities. The elements of each vector  $b$  were registered over 5 seconds. This means that if an element of  $b$  is a sum or a difference of  $n$  projectors the measurement for each of the  $n$  projectors took  $5/n$  seconds. In this way the measurements for observation vectors

of the same length take the same amount of time. To obtain the frequencies we can divide these values by the total number of photon coincidences counted or by a sum of coincidences counted for a set of projectors forming a basis. The set of such projectors is not unique. In our calculations we use the unnormalized coincidences and normalize the reconstructed density matrices.

### Standard 36 state tomography

$$\bar{b}_S = \begin{bmatrix} 2727 & 2575 & 2844 & 1448 & 127 & 193 & 25 & 2955 & 40 & 27 & 1264 & 809 & 1231 & 2762 & 3831 & 113 & 112 \\ 30 & 58 & 116 & 1312 & 2457 & 2364 & 3928 & 72 & 2555 & 2375 & 863 & 1263 & 757 & 2722 & 2773 & 3452 & 4102 \\ 1244 & 1401 & 1890 & 2688 & 826 & 1483 & 2159 & 1096 & 1152 & 1386 & 2126 & 40 & 50 & 2251 & 4529 & 1758 & 2012 \\ 1461 & 1194 & 1001 & 37 & 1772 & 956 & 1713 & 1758 & 1349 & 1010 & 51 & 2178 & 1945 & 3434 & 2090 & 2043 & 2310 \\ 1270 & 1697 & 1865 & 1224 & 1120 & 722 & 2102 & 1407 & 1433 & 1210 & 1150 & 1200 & 1057 & 5667 & 266 & 2409 & 2782 \\ 1581 & 1216 & 1383 & 1643 & 1302 & 1692 & 1764 & 1624 & 776 & 995 & 1132 & 778 & 934 & 21 & 6227 & 991 & 1250 \\ 126 & 43 & 61 & 648 & 2282 & 2660 & 13 & 23 & 1892 & 2199 & 1277 & 895 & 1141 & 977 & 347 & 1887 & 1295 \\ 2706 & 2747 & 2426 & 1751 & 14 & 36 & 35 & 2274 & 8 & 26 & 928 & 1240 & 888 & 802 & 310 & 17 & 23 \\ 1403 & 1448 & 1248 & 113 & 1051 & 1095 & 10 & 1134 & 951 & 1399 & 35 & 2079 & 2034 & 646 & 352 & 974 & 719 \\ 1440 & 1328 & 1144 & 2204 & 1101 & 1547 & 49 & 1175 & 1012 & 969 & 2174 & 63 & 36 & 1224 & 216 & 887 & 602 \\ 940 & 1611 & 907 & 1238 & 1253 & 1422 & 11 & 1235 & 1018 & 1069 & 1099 & 756 & 1067 & 1769 & 9 & 852 & 664 \\ 1798 & 1108 & 1501 & 950 & 1197 & 1398 & 33 & 1001 & 978 & 1447 & 953 & 1452 & 1074 & 31 & 601 & 1085 & 718 \\ 1316 & 1304 & 1837 & 1250 & 1385 & 1781 & 42 & 1458 & 952 & 1172 & 1147 & 710 & 1251 & 901 & 1634 & 939 & 651 \\ 1607 & 1537 & 981 & 1279 & 1149 & 920 & 1594 & 1156 & 1207 & 1065 & 991 & 1268 & 691 & 1085 & 987 & 1753 & 1986 \\ 42 & 2845 & 1706 & 1231 & 1225 & 2556 & 962 & 1090 & 32 & 1482 & 996 & 1111 & 1012 & 790 & 1732 & 81 & 208 \\ 2740 & 40 & 967 & 1276 & 1273 & 87 & 684 & 1568 & 2169 & 886 & 1160 & 819 & 880 & 1359 & 755 & 2663 & 2424 \\ 1354 & 1497 & 107 & 25 & 25 & 1165 & 1024 & 2671 & 1050 & 2240 & 2215 & 1949 & 64 & 2083 & 131 & 1545 & 1485 \\ 1298 & 1459 & 2689 & 2352 & 2356 & 1818 & 564 & 43 & 876 & 156 & 47 & 72 & 1866 & 5 & 2458 & 1053 & 938 \\ 1266 & 1095 & 914 & 780 & 1014 & 1010 & 4 & 1130 & 976 & 1145 & 1357 & 1103 & 1129 & 2815 & 2720 & 971 & 688 \\ 1231 & 1320 & 1485 & 1593 & 1099 & 1223 & 1947 & 1209 & 1265 & 1323 & 877 & 1205 & 977 & 2489 & 2139 & 1915 & 2175 \\ 2459 & 57 & 1288 & 1250 & 791 & 28 & 1043 & 1137 & 2090 & 1251 & 1081 & 944 & 1118 & 2145 & 3266 & 2585 & 2534 \\ 50 & 2308 & 1075 & 1066 & 1371 & 2133 & 923 & 1163 & 80 & 1034 & 1038 & 1332 & 1207 & 3415 & 1442 & 192 & 342 \\ 818 & 1591 & 2448 & 2275 & 2158 & 947 & 875 & 22 & 1305 & 22 & 39 & 31 & 2170 & 5417 & 141 & 1841 & 1860 \\ 1833 & 767 & 65 & 86 & 28 & 1098 & 949 & 2281 & 859 & 2336 & 1999 & 2091 & 28 & 38 & 4777 & 1096 & 1077 \\ 1229 & 1498 & 1585 & 2277 & 712 & 772 & 2 & 1617 & 689 & 979 & 80 & 2142 & 61 & 1173 & 1991 & 601 & 314 \\ 1259 & 1048 & 878 & 158 & 1535 & 1390 & 2521 & 804 & 1576 & 1348 & 2087 & 66 & 1988 & 1094 & 1532 & 2478 & 2874 \\ 1743 & 924 & 123 & 1133 & 2117 & 918 & 1288 & 2314 & 1521 & 60 & 1199 & 856 & 799 & 994 & 2446 & 1994 & 2063 \\ 850 & 1559 & 2345 & 1188 & 213 & 1343 & 1326 & 81 & 703 & 2252 & 866 & 1327 & 1284 & 1313 & 981 & 999 & 1180 \\ 2423 & 84 & 1608 & 1713 & 1499 & 2127 & 1416 & 936 & 189 & 970 & 718 & 914 & 1206 & 2181 & 142 & 455 & 725 \\ 199 & 2354 & 828 & 733 & 902 & 34 & 1028 & 1672 & 1919 & 1103 & 1253 & 1332 & 677 & 12 & 3277 & 2470 & 2414 \\ 1691 & 1357 & 1323 & 92 & 1424 & 1634 & 31 & 1291 & 881 & 1002 & 2036 & 64 & 1885 & 2699 & 2757 & 1040 & 852 \\ 1331 & 1459 & 1514 & 2563 & 1170 & 1148 & 1696 & 1372 & 1081 & 1267 & 23 & 2185 & 86 & 2546 & 1817 & 1481 & 1784 \\ 1648 & 1243 & 2746 & 1707 & 30 & 1217 & 1114 & 42 & 991 & 2140 & 1068 & 946 & 939 & 2106 & 2968 & 1278 & 1244 \\ 1327 & 1561 & 79 & 899 & 2552 & 1460 & 626 & 2535 & 1140 & 52 & 1036 & 1158 & 1040 & 3398 & 1413 & 1354 & 1335 \\ 48 & 2814 & 1524 & 1198 & 1435 & 84 & 889 & 1204 & 2062 & 804 & 913 & 746 & 1349 & 5230 & 157 & 2610 & 2403 \\ 2812 & 27 & 1327 & 1275 & 1066 & 2657 & 796 & 1432 & 32 & 1483 & 1151 & 1255 & 768 & 27 & 4284 & 47 & 85 \end{bmatrix}$$

The rows of the observation vector  $\bar{b}_S$  correspond to the following consecutive projectors:  $|HH\rangle\langle HH|$ ,  $|HV\rangle\langle HV|$ ,  $|HD\rangle\langle HD|$ ,  $|HA\rangle\langle HA|$ ,  $|HL\rangle\langle HL|$ ,  $|HR\rangle\langle HR|$ ,  $|VH\rangle\langle VH|$ ,  $|VV\rangle\langle VV|$ ,  $|VD\rangle\langle VD|$ ,  $|VA\rangle\langle VA|$ ,  $|VL\rangle\langle VL|$ ,  $|VR\rangle\langle VR|$ ,  $|DH\rangle\langle DH|$ ,  $|DV\rangle\langle DV|$ ,  $|DD\rangle\langle DD|$ ,  $|DA\rangle\langle DA|$ ,  $|DL\rangle\langle DL|$ ,  $|DR\rangle\langle DR|$ ,  $|AH\rangle\langle AH|$ ,  $|AV\rangle\langle AV|$ ,  $|AD\rangle\langle AD|$ ,  $|AA\rangle\langle AA|$ ,  $|AL\rangle\langle AL|$ ,  $|AR\rangle\langle AR|$ ,  $|LH\rangle\langle LH|$ ,  $|LV\rangle\langle LV|$ ,  $|LD\rangle\langle LD|$ ,  $|LA\rangle\langle LA|$ ,  $|LL\rangle\langle LL|$ ,  $|LR\rangle\langle LR|$ ,  $|RH\rangle\langle RH|$ ,  $|RV\rangle\langle RV|$ ,  $|RD\rangle\langle RD|$ ,  $|RA\rangle\langle RA|$ ,  $|RL\rangle\langle RL|$ ,  $|RR\rangle\langle RR|$ .

## JKMW tomography

$$\bar{b}_J = \begin{bmatrix} 2727 & 2575 & 2844 & 1448 & 127 & 193 & 25 & 2955 & 40 & 27 & 1264 & 809 & 1231 & 2762 & 3831 & 113 & 112 \\ 30 & 58 & 116 & 1312 & 2457 & 2364 & 3928 & 72 & 2555 & 2375 & 863 & 1263 & 757 & 2722 & 2773 & 3452 & 4102 \\ 1244 & 1401 & 1890 & 2688 & 826 & 1483 & 2159 & 1096 & 1152 & 1386 & 2126 & 40 & 50 & 2251 & 4529 & 1758 & 2012 \\ 1270 & 1697 & 1865 & 1224 & 1120 & 722 & 2102 & 1407 & 1433 & 1210 & 1150 & 1200 & 1057 & 5667 & 266 & 2409 & 2782 \\ 126 & 43 & 61 & 648 & 2282 & 2660 & 13 & 23 & 1892 & 2199 & 1277 & 895 & 1141 & 977 & 347 & 1887 & 1295 \\ 2706 & 2747 & 2426 & 1751 & 14 & 36 & 35 & 2274 & 8 & 26 & 928 & 1240 & 888 & 802 & 310 & 17 & 23 \\ 1403 & 1448 & 1248 & 113 & 1051 & 1095 & 10 & 1134 & 951 & 1399 & 35 & 2079 & 2034 & 646 & 352 & 974 & 719 \\ 940 & 1611 & 907 & 1238 & 1253 & 1422 & 11 & 1235 & 1018 & 1069 & 1099 & 756 & 1067 & 1769 & 9 & 852 & 664 \\ 1691 & 1357 & 1323 & 92 & 1424 & 1634 & 31 & 1291 & 881 & 1002 & 2036 & 64 & 1885 & 2699 & 2757 & 1040 & 852 \\ 1331 & 1459 & 1514 & 2563 & 1170 & 1148 & 1696 & 1372 & 1081 & 1267 & 23 & 2185 & 86 & 2546 & 1817 & 1481 & 1784 \\ 1648 & 1243 & 2746 & 1707 & 30 & 1217 & 1114 & 42 & 991 & 2140 & 1068 & 946 & 939 & 2106 & 2968 & 1278 & 1244 \\ 48 & 2814 & 1524 & 1198 & 1435 & 84 & 889 & 1204 & 2062 & 804 & 913 & 746 & 1349 & 5230 & 157 & 2610 & 2403 \\ 1316 & 1304 & 1837 & 1250 & 1385 & 1781 & 42 & 1458 & 952 & 1172 & 1147 & 710 & 1251 & 901 & 1634 & 939 & 651 \\ 1607 & 1537 & 981 & 1279 & 1149 & 920 & 1594 & 1156 & 1207 & 1065 & 991 & 1268 & 691 & 1085 & 987 & 1753 & 1986 \\ 42 & 2845 & 1706 & 1231 & 1225 & 2556 & 962 & 1090 & 32 & 1482 & 996 & 1111 & 1012 & 790 & 1732 & 81 & 208 \\ 1298 & 1459 & 2689 & 2352 & 2356 & 1818 & 564 & 43 & 876 & 156 & 47 & 72 & 1866 & 5 & 2458 & 1053 & 938 \end{bmatrix}$$

The rows of the observation vector  $\bar{b}_J$  correspond to the following consecutive projectors:  $|HH\rangle\langle HH|$ ,  $|HV\rangle\langle HV|$ ,  $|HD\rangle\langle HD|$ ,  $|HL\rangle\langle HL|$ ,  $|VH\rangle\langle VH|$ ,  $|VV\rangle\langle VV|$ ,  $|VD\rangle\langle VD|$ ,  $|VL\rangle\langle VL|$ ,  $|RH\rangle\langle RH|$ ,  $|RV\rangle\langle RV|$ ,  $|RD\rangle\langle RD|$ ,  $|RL\rangle\langle RL|$ ,  $|DH\rangle\langle DH|$ ,  $|DV\rangle\langle DV|$ ,  $|DD\rangle\langle DD|$ ,  $|DR\rangle\langle DR|$ .

## MUB-based tomography

$$\bar{b}_M = \begin{bmatrix} 1316 & 1304 & 1837 & 1250 & 1385 & 1781 & 42 & 1458 & 952 & 1172 & 1147 & 710 & 1251 & 901 & 1634 & 939 & 651 \\ 1607 & 1537 & 981 & 1279 & 1149 & 920 & 1594 & 1156 & 1207 & 1065 & 991 & 1268 & 691 & 1085 & 987 & 1753 & 1986 \\ 1266 & 1095 & 914 & 780 & 1014 & 1010 & 4 & 1130 & 976 & 1145 & 1357 & 1103 & 1129 & 2815 & 2720 & 971 & 688 \\ 1231 & 1320 & 1485 & 1593 & 1099 & 1223 & 1947 & 1209 & 1265 & 1323 & 877 & 1205 & 977 & 2489 & 2139 & 1915 & 2175 \\ 1743 & 924 & 123 & 1133 & 2117 & 918 & 1288 & 2314 & 1521 & 60 & 1199 & 856 & 799 & 994 & 2446 & 1994 & 2063 \\ 850 & 1559 & 2345 & 1188 & 213 & 1343 & 1326 & 81 & 703 & 2252 & 866 & 1327 & 1284 & 1313 & 981 & 999 & 1180 \\ 1648 & 1243 & 2746 & 1707 & 30 & 1217 & 1114 & 42 & 991 & 2140 & 1068 & 946 & 939 & 2106 & 2968 & 1278 & 1244 \\ 1327 & 1561 & 79 & 899 & 2552 & 1460 & 626 & 2535 & 1140 & 52 & 1036 & 1158 & 1040 & 3398 & 1413 & 1354 & 1335 \\ 1798 & 1108 & 1501 & 950 & 1197 & 1398 & 33 & 1001 & 978 & 1447 & 953 & 1452 & 1074 & 31 & 601 & 1085 & 718 \\ 940 & 1611 & 907 & 1238 & 1253 & 1422 & 11 & 1235 & 1018 & 1069 & 1099 & 756 & 1067 & 1769 & 9 & 852 & 664 \\ 1581 & 1216 & 1383 & 1643 & 1302 & 1692 & 1764 & 1624 & 776 & 995 & 1132 & 778 & 934 & 21 & 6227 & 991 & 1250 \\ 1270 & 1697 & 1865 & 1224 & 1120 & 722 & 2102 & 1407 & 1433 & 1210 & 1150 & 1200 & 1057 & 5667 & 266 & 2409 & 2782 \\ 97 & 5284 & 2720 & 1181 & 135 & 134 & 75 & 2337 & 16 & 23 & 1323 & 958 & 1438 & 2600 & 1867 & 23 & 21 \\ 5418 & 98 & 2143 & 874 & 119 & 27 & 133 & 2943 & 133 & 31 & 1279 & 1095 & 1085 & 957 & 2362 & 277 & 268 \\ 32 & 55 & 87 & 1558 & 3494 & 4939 & 1892 & 88 & 175 & 2121 & 1091 & 868 & 1002 & 826 & 1537 & 586 & 623 \\ 157 & 27 & 109 & 478 & 1725 & 253 & 1887 & 32 & 4213 & 2268 & 1328 & 775 & 1148 & 2240 & 853 & 4544 & 4390 \\ 2022 & 1093 & 184 & 120 & 182 & 1636 & 1011 & 2320 & 786 & 1912 & 4230 & 57 & 48 & 607 & 2921 & 944 & 945 \\ 1245 & 851 & 111 & 130 & 41 & 646 & 637 & 2232 & 936 & 2583 & 52 & 4028 & 9 & 693 & 1795 & 931 & 998 \\ 1404 & 1117 & 1788 & 40 & 2693 & 1246 & 990 & 60 & 1415 & 71 & 43 & 70 & 3875 & 2676 & 868 & 1920 & 1922 \\ 1355 & 1652 & 3361 & 4078 & 1349 & 1156 & 613 & 115 & 862 & 81 & 13 & 84 & 54 & 2240 & 1613 & 868 & 921 \end{bmatrix}$$

The rows of the observation vector  $\bar{b}_M$  correspond to the following consecutive projectors:  $|DH\rangle\langle DH|$ ,  $|DV\rangle\langle DV|$ ,  $|AH\rangle\langle AH|$ ,  $|AV\rangle\langle AV|$ ,  $|LD\rangle\langle LD|$ ,  $|LA\rangle\langle LA|$ ,  $|RD\rangle\langle RD|$ ,  $|RA\rangle\langle RA|$ ,  $|VR\rangle\langle VR|$ ,  $|VL\rangle\langle VL|$ ,  $|HR\rangle\langle HR|$ ,  $|HL\rangle\langle HL|$ ,  $|\Phi^+\rangle\langle\Phi^+|$ ,  $|\Phi^-\rangle\langle\Phi^-|$ ,  $|\Psi^+\rangle\langle\Psi^+|$ ,  $|\Psi^-\rangle\langle\Psi^-|$ ,  $\frac{1}{2}(|DL\rangle+i|AR\rangle)\langle(DL-i|AR|)$ ,  $\frac{1}{2}(|DL\rangle-i|AR\rangle)\langle(DL+i|AR|)$ ,  $\frac{1}{2}(|DR\rangle+i|AL\rangle)\langle(DR-i|AL|)$ ,  $\frac{1}{2}(|DR\rangle-i|AL\rangle)\langle(DR+i|AL|)$ , where  $|\Phi^\pm\rangle = (|HH\rangle \pm |VV\rangle)/\sqrt{2}$  and  $|\Psi^\pm\rangle = (|HV\rangle \pm |VH\rangle)/\sqrt{2}$ .

## Optimal tomography

$$\bar{b}_O = \begin{bmatrix} 2727 & 2575 & 2844 & 1448 & 127 & 193 & 25 & 2955 & 40 & 27 & 1264 & 809 & 1231 & 2762 & 3831 & 113 & 112 \\ 30 & 58 & 116 & 1312 & 2457 & 2364 & 3928 & 72 & 2555 & 2375 & 863 & 1263 & 757 & 2722 & 2773 & 3452 & 4102 \\ 126 & 43 & 61 & 648 & 2282 & 2660 & 13 & 23 & 1892 & 2199 & 1277 & 895 & 1141 & 977 & 347 & 1887 & 1295 \\ 2706 & 2747 & 2426 & 1751 & 14 & 36 & 35 & 2274 & 8 & 26 & 928 & 1240 & 888 & 802 & 310 & 17 & 23 \\ \overline{108} & 103 & 444 & 1325 & \overline{473} & 263 & 223 & \overline{331} & \overline{98} & 188 & 1037 & \overline{1069} & 947 & \overline{591} & 1219 & \overline{142} & \overline{149} \\ \overline{155} & 240 & 241 & \overline{209} & \overline{91} & \overline{485} & 169 & \overline{108} & 328 & 107 & 9 & 211 & 61 & 2823 & \overline{2980} & 709 & 766 \\ 25 & 104 & 461 & 235 & 185 & 385 & 19 & 164 & \overline{12} & 13 & \overline{105} & \overline{196} & 61 & \overline{957} & \overline{543} & \overline{16} & \overline{18} \\ \overline{231} & 70 & 131 & 1092 & \overline{356} & \overline{431} & \overline{14} & 163 & \overline{96} & \overline{11} & \overline{978} & 1039 & \overline{912} & \overline{763} & 383 & 219 & \overline{269} \\ \overline{18} & 60 & 52 & \overline{1045} & 25 & 226 & \overline{19} & 20 & 30 & 215 & \overline{1069} & 1008 & 999 & 289 & 68 & 43 & 58 \\ \overline{429} & 251 & 297 & 144 & 28 & 12 & \overline{11} & 117 & 20 & \overline{189} & 73 & 348 & 3 & 869 & 296 & \overline{116} & 27 \\ 188 & 108 & 252 & \overline{157} & 25 & \overline{151} & \overline{176} & \overline{26} & 29 & \overline{129} & 57 & 31 & \overline{143} & \overline{702} & 576 & \overline{81} & 94 \\ \overline{36} & \overline{205} & 318 & \overline{1202} & 182 & 121 & 412 & \overline{284} & 247 & 40 & 1032 & \overline{1059} & 951 & \overline{726} & \overline{142} & 498 & 545 \\ \overline{62} & 13 & \overline{11} & 540 & 884 & 2342 & 2 & 27 & \overline{2019} & \overline{73} & \overline{118} & 46 & \overline{73} & \overline{706} & 341 & \overline{1979} & \overline{1883} \\ 1 & \overline{0} & 14 & 957 & 2060 & 393 & \overline{151} & 7 & \overline{4} & \overline{2158} & \overline{978} & 949 & 799 & 918 & 634 & 52 & 56 \\ \overline{2660} & 2593 & 288 & 153 & 8 & 53 & 28 & \overline{302} & 58 & \overline{4} & 21 & 68 & 176 & 821 & 247 & \overline{127} & \overline{123} \\ 48 & \overline{10} & \overline{2468} & \overline{1111} & 38 & 93 & \overline{11} & 2501 & \overline{18} & \overline{42} & 1153 & 1010 & \overline{1172} & \overline{482} & 390 & 6 & 85 \end{bmatrix}$$

The negative elements of  $\bar{b}_O$  are marked with an overline. The rows of the observation vector  $\bar{b}_O$  correspond to the following consecutive measurements:  $|HH\rangle\langle HH|$ ,  $|HV\rangle\langle HV|$ ,  $|VV\rangle\langle VV|$ ,  $|HD\rangle\langle HD| - |HA\rangle\langle HA|$ ,  $|HL\rangle\langle HL| - |HR\rangle\langle HR|$ ,  $|DH\rangle\langle DH| - |AH\rangle\langle AH|$ ,  $|LH\rangle\langle LH| - |RH\rangle\langle RH|$ ,  $|VD\rangle\langle VD| - |VA\rangle\langle VA|$ ,  $|VL\rangle\langle VL| - |VR\rangle\langle VR|$ ,  $|DV\rangle\langle DV| - |AV\rangle\langle AV|$ ,  $|LV\rangle\langle LV| - |RV\rangle\langle RV|$ ,  $|\Psi^+\rangle\langle\Psi^+| - |\Psi^-\rangle\langle\Psi^-|$ ,  $|\bar{\Psi}^+\rangle\langle\bar{\Psi}^+| - |\bar{\Psi}^-\rangle\langle\bar{\Psi}^-|$ ,  $|\Phi^+\rangle\langle\Phi^+| - |\Phi^-\rangle\langle\Phi^-|$ ,  $|\bar{\Phi}^+\rangle\langle\bar{\Phi}^+| - |\bar{\Phi}^-\rangle\langle\bar{\Phi}^-|$ , where  $|\bar{\Phi}^\pm\rangle = (|HH\rangle \pm i|VV\rangle)/\sqrt{2}$  and  $|\bar{\Psi}^\pm\rangle = (|HV\rangle \pm i|VH\rangle)/\sqrt{2}$ .

## Pauli matrices based tomography

$$\bar{b}_P = \begin{bmatrix} \overline{1277} & 1264 & 132 & \overline{57} & 133 & 1144 & 40 & \overline{113} & \overline{1037} & 95 & \overline{52} & 170 & 55 & 175 & 212 & \overline{1244} & \overline{1102} \\ 268 & \overline{197} & \overline{1241} & \overline{1129} & \overline{1115} & \overline{126} & 134 & 1222 & \overline{68} & 1100 & 1032 & 984 & \overline{986} & \overline{825} & 577 & \overline{63} & \overline{59} \\ \overline{82} & \overline{2} & 357 & 196 & 80 & 269 & 98 & 95 & 9 & 71 & \overline{81} & \overline{114} & 102 & \overline{128} & 17 & 33 & 38 \\ 107 & 107 & 105 & 39 & 105 & 117 & \overline{79} & 69 & \overline{21} & 58 & 24 & \overline{83} & \overline{41} & \overline{830} & \overline{560} & 49 & \overline{57} \\ 143 & \overline{79} & \overline{1222} & \overline{216} & 1107 & \overline{46} & \overline{132} & 1182 & 242 & \overline{1070} & 75 & \overline{65} & \overline{96} & 243 & \overline{23} & 268 & 244 \\ 1247 & \overline{1264} & 146 & 264 & 57 & 1167 & 74 & \overline{127} & \overline{940} & 137 & \overline{74} & 23 & \overline{13} & \overline{759} & 248 & \overline{1145} & \overline{1002} \\ \overline{98} & 138 & 225 & 1148 & \overline{269} & \overline{276} & \overline{214} & 224 & \overline{172} & \overline{26} & \overline{1005} & 1049 & \overline{932} & 19 & \overline{120} & \overline{359} & 407 \\ \overline{134} & \overline{68} & \overline{94} & \overline{55} & \overline{87} & \overline{155} & 199 & \overline{61} & 76 & 15 & 27 & \overline{10} & 20 & \overline{745} & \overline{263} & 140 & 138 \\ 45 & 22 & 196 & 1186 & \overline{224} & 245 & 121 & \overline{155} & 34 & \overline{14} & 1054 & \overline{1039} & \overline{973} & 151 & 576 & 93 & \overline{104} \\ 137 & \overline{6} & 269 & \overline{177} & \overline{60} & \overline{249} & 90 & \overline{113} & 154 & 148 & 32 & 280 & 33 & 977 & \overline{1342} & 413 & 397 \\ 1319 & 1305 & 1273 & 310 & \overline{1150} & \overline{1199} & \overline{970} & 1284 & \overline{1100} & \overline{1130} & 13 & \overline{27} & 55 & 34 & 255 & \overline{1302} & \overline{1316} \\ \overline{19} & 39 & 118 & 90 & 72 & \overline{35} & 976 & 183 & 174 & 44 & \overline{20} & \overline{16} & \overline{10} & 926 & 1487 & 415 & 724 \\ \overline{64} & 82 & 248 & 140 & \overline{249} & 19 & 102 & \overline{176} & \overline{65} & 202 & \overline{16} & \overline{31} & 26 & \overline{440} & 644 & \overline{50} & \overline{45} \\ \overline{292} & 246 & \overline{28} & \overline{33} & \overline{32} & \overline{237} & 79 & 4 & 174 & \overline{41} & 41 & \overline{69} & 29 & 1846 & \overline{1638} & 296 & 370 \\ 29 & \overline{47} & 91 & \overline{242} & \overline{16} & 113 & \overline{981} & 158 & \overline{158} & \overline{44} & 188 & \overline{200} & 182 & 54 & 274 & \overline{367} & \overline{680} \\ 1397 & 1356 & 1362 & 1290 & 1220 & 1313 & 1000 & 1331 & 1124 & 1157 & 1083 & 1052 & 1004 & 1816 & 1815 & 1367 & 1383 \end{bmatrix}$$

The negative elements of  $\bar{b}_P$  are marked with an overline. The rows of the observation vector  $\bar{b}_P$  correspond to the following consecutive measurements:  $(|DD\rangle\langle DD| + |AA\rangle\langle AA|) - (|DA\rangle\langle DA| + |AD\rangle\langle AD|)$ ,  $(|DL\rangle\langle DL| + |AR\rangle\langle AR|) - (|DR\rangle\langle DR| + |AL\rangle\langle AL|)$ ,  $(|DH\rangle\langle DH| + |AV\rangle\langle AV|) - (|DV\rangle\langle DV| + |AH\rangle\langle AH|)$ ,  $(|DH\rangle\langle DH| + |AH\rangle\langle AH|) - (|DV\rangle\langle DV| + |AV\rangle\langle AV|)$ ,  $(|LD\rangle\langle LD| + |RA\rangle\langle RA|) - (|LA\rangle\langle LA| + |RD\rangle\langle RD|)$ ,  $(|LL\rangle\langle LL| + |RR\rangle\langle RR|) - (|LR\rangle\langle LR| + |RL\rangle\langle RL|)$ ,  $(|LH\rangle\langle LH| + |RV\rangle\langle RV|) - (|LV\rangle\langle LV| + |RH\rangle\langle RH|)$ ,  $(|LH\rangle\langle LH| + |RH\rangle\langle RH|) - (|LV\rangle\langle LV| + |RV\rangle\langle RV|)$ ,  $(|HD\rangle\langle HD| + |VA\rangle\langle VA|) - (|HA\rangle\langle HA| + |VD\rangle\langle VD|)$ ,  $(|HL\rangle\langle HL| + |VR\rangle\langle VR|) - (|HR\rangle\langle HR| + |VL\rangle\langle VL|)$ ,  $(|HH\rangle\langle HH| + |VV\rangle\langle VV|) - (|HV\rangle\langle HV| + |VH\rangle\langle VH|)$ ,  $(|HH\rangle\langle HH| + |VH\rangle\langle VH|) - (|HV\rangle\langle HV| + |VV\rangle\langle VV|)$ ,  $(|HD\rangle\langle HD| - |HA\rangle\langle HA|) + (|VD\rangle\langle VD| - |VA\rangle\langle VA|)$ ,  $(|HL\rangle\langle HL| - |HR\rangle\langle HR|) + (|VL\rangle\langle VL| - |VR\rangle\langle VR|)$ ,  $(|HH\rangle\langle HH| - |HV\rangle\langle HV|) + (|VH\rangle\langle VH| - |VV\rangle\langle VV|)$ ,  $(|HH\rangle\langle HH| + |HV\rangle\langle HV|) + (|VH\rangle\langle VH| + |VV\rangle\langle VV|)$ .

## Error analysis

### Estimated variances

For all the tomographies the vectors of variances for the 17 measured states are given as matrices

$$\sigma^2(b) = \begin{matrix} & \rho_1 & \rho_2 & \dots & \rho_{17} \\ \begin{matrix} b_1 \\ b_2 \\ \vdots \\ b_N \end{matrix} & \begin{bmatrix} \sigma^2(b_{1,1}) & \sigma^2(b_{1,2}) & \dots & \sigma^2(b_{1,17}) \\ \sigma^2(b_{2,1}) & \sigma^2(b_{2,2}) & \dots & \sigma^2(b_{2,17}) \\ \vdots & \vdots & \ddots & \vdots \\ \sigma^2(b_{N,1}) & \sigma^2(b_{N,2}) & \dots & \sigma^2(b_{N,17}) \end{bmatrix} \end{matrix}.$$

They can be approximated directly with  $\sigma^2(b) \approx \sigma^2(\bar{b}) = \bar{b}$  for all the tomographies except the optimal one and the tomography based on the Pauli matrices. For the optimal tomography the matrix of variances reads

$$\sigma^2(b_O) = \begin{bmatrix} 2727 & 2575 & 2844 & 1448 & 127 & 193 & 25 & 2955 & 40 & 27 & 1264 & 809 & 1231 & 2762 & 3831 & 113 & 112 \\ 30 & 58 & 116 & 1312 & 2457 & 2364 & 3928 & 72 & 2555 & 2375 & 863 & 1263 & 757 & 2722 & 2773 & 3452 & 4102 \\ 126 & 43 & 61 & 648 & 2282 & 2660 & 13 & 23 & 1892 & 2199 & 1277 & 895 & 1141 & 977 & 347 & 1887 & 1295 \\ 2706 & 2747 & 2426 & 1751 & 14 & 36 & 35 & 2274 & 8 & 26 & 928 & 1240 & 888 & 802 & 310 & 17 & 23 \\ 1352 & 1297 & 1445 & 1362 & 1299 & 1219 & 1936 & 1427 & 1250 & 1198 & 1088 & 1109 & 997 & 2842 & 3309 & 1900 & 2161 \\ 1425 & 1456 & 1624 & 1433 & 1211 & 1207 & 1933 & 1515 & 1104 & 1102 & 1141 & 989 & 995 & 2844 & 3246 & 1700 & 2016 \\ 1291 & 1199 & 1375 & 1015 & 1199 & 1395 & 23 & 1294 & 964 & 1158 & 1252 & 906 & 1190 & 1858 & 2177 & 955 & 669 \\ 1460 & 1427 & 1454 & 1184 & 1068 & 1203 & 16 & 1454 & 785 & 990 & 1058 & 1103 & 973 & 1936 & 2374 & 820 & 583 \\ 1421 & 1388 & 1196 & 1158 & 1076 & 1321 & 29 & 1154 & 981 & 1184 & 1104 & 1071 & 1035 & 935 & 284 & 930 & 660 \\ 1369 & 1359 & 1204 & 1094 & 1225 & 1410 & 22 & 1118 & 998 & 1258 & 1026 & 1104 & 1070 & 900 & 305 & 968 & 691 \\ 1419 & 1428 & 1233 & 1436 & 1124 & 1071 & 1770 & 1182 & 1236 & 1194 & 934 & 1236 & 834 & 1787 & 1563 & 1834 & 2080 \\ 1295 & 1253 & 1196 & 1360 & 1352 & 1269 & 2108 & 1088 & 1328 & 1307 & 1055 & 1125 & 1037 & 1820 & 1674 & 1979 & 2329 \\ 94 & 41 & 98 & 1018 & 2609 & 2596 & 1889 & 60 & 2194 & 2195 & 1209 & 821 & 1075 & 1533 & 1195 & 2565 & 2506 \\ 44 & 53 & 146 & 1065 & 2112 & 2196 & 1772 & 86 & 2074 & 2276 & 1031 & 1114 & 862 & 1685 & 1628 & 2274 & 2316 \\ 2757 & 2691 & 2431 & 1027 & 127 & 80 & 104 & 2640 & 74 & 27 & 1301 & 1026 & 1262 & 1778 & 2115 & 150 & 144 \\ 2806 & 2583 & 2521 & 1249 & 160 & 164 & 105 & 2580 & 55 & 67 & 1183 & 1049 & 1227 & 1737 & 1964 & 306 & 274 \end{bmatrix}.$$

For the Pauli matrices based tomography the matrix of variances reads

$$\sigma^2(b_P) = \begin{bmatrix} 1323 & 1313 & 1259 & 1206 & 1165 & 1201 & 903 & 1240 & 1093 & 1163 & 1069 & 1052 & 1054 & 1927 & 1799 & 1380 & 1377 \\ 1326 & 1329 & 1327 & 1185 & 1142 & 1257 & 853 & 1254 & 1022 & 1189 & 1075 & 1036 & 1032 & 1886 & 1877 & 1384 & 1340 \\ 1355 & 1314 & 1304 & 1225 & 1162 & 1234 & 897 & 1238 & 1100 & 1176 & 1093 & 1072 & 1012 & 1823 & 1870 & 1395 & 1375 \\ 1355 & 1314 & 1304 & 1225 & 1162 & 1234 & 897 & 1238 & 1100 & 1176 & 1093 & 1072 & 1012 & 1823 & 1870 & 1395 & 1375 \\ 1392 & 1322 & 1323 & 1232 & 1228 & 1235 & 1089 & 1243 & 1089 & 1126 & 1042 & 1072 & 1016 & 1953 & 1952 & 1406 & 1455 \\ 1370 & 1320 & 1322 & 1230 & 1225 & 1225 & 1032 & 1311 & 1051 & 1090 & 1009 & 1062 & 1000 & 1863 & 1965 & 1396 & 1407 \\ 1378 & 1341 & 1325 & 1273 & 1210 & 1236 & 1062 & 1271 & 1057 & 1149 & 1056 & 1114 & 1005 & 1878 & 2024 & 1400 & 1456 \\ 1378 & 1341 & 1325 & 1273 & 1210 & 1236 & 1062 & 1271 & 1057 & 1149 & 1056 & 1114 & 1005 & 1878 & 2024 & 1400 & 1456 \\ 1387 & 1343 & 1321 & 1261 & 1188 & 1270 & 983 & 1291 & 1116 & 1191 & 1097 & 1090 & 1016 & 1889 & 1797 & 1416 & 1411 \\ 1397 & 1408 & 1414 & 1264 & 1218 & 1309 & 978 & 1317 & 1051 & 1180 & 1084 & 1047 & 1033 & 1872 & 1776 & 1334 & 1354 \\ 1397 & 1356 & 1362 & 1290 & 1220 & 1313 & 1000 & 1331 & 1124 & 1157 & 1083 & 1052 & 1004 & 1816 & 1815 & 1367 & 1383 \\ 1397 & 1356 & 1362 & 1290 & 1220 & 1313 & 1000 & 1331 & 1124 & 1157 & 1083 & 1052 & 1004 & 1816 & 1815 & 1367 & 1383 \\ 1387 & 1343 & 1321 & 1261 & 1188 & 1270 & 983 & 1291 & 1116 & 1191 & 1097 & 1090 & 1016 & 1889 & 1797 & 1416 & 1411 \\ 1397 & 1408 & 1414 & 1264 & 1218 & 1309 & 978 & 1317 & 1051 & 1180 & 1084 & 1047 & 1033 & 1872 & 1776 & 1334 & 1354 \\ 1397 & 1356 & 1362 & 1290 & 1220 & 1313 & 1000 & 1331 & 1124 & 1157 & 1083 & 1052 & 1004 & 1816 & 1815 & 1367 & 1383 \\ 1397 & 1356 & 1362 & 1290 & 1220 & 1313 & 1000 & 1331 & 1124 & 1157 & 1083 & 1052 & 1004 & 1816 & 1815 & 1367 & 1383 \end{bmatrix}.$$

### Estimated error radii

For each tomography and reconstructed state we have estimated the maximum error  $R$  as described in the main text. Our results are summarized in the following matrix:

$$R = \begin{array}{c} \rho_1 \\ \rho_2 \\ \rho_3 \\ \rho_4 \\ \rho_5 \\ \rho_6 \\ \rho_7 \\ \rho_8 \\ \rho_9 \\ \rho_{10} \\ \rho_{11} \\ \rho_{12} \\ \rho_{13} \\ \rho_{14} \\ \rho_{15} \\ \rho_{16} \\ \rho_{17} \end{array} \begin{array}{ccccc} \text{Optimal} & \text{MUB} & \text{Standard} & \text{Pauli} & \text{JKMW} \\ \left[ \begin{array}{ccccc} 0.0983 & 0.1475 & 0.2183 & 0.2407 & 0.5712 \\ 0.0997 & 0.1554 & 0.2221 & 0.2448 & 0.5357 \\ 0.0987 & 0.1506 & 0.2231 & 0.2422 & 0.5297 \\ 0.0997 & 0.1477 & 0.2130 & 0.2304 & 0.5044 \\ 0.1051 & 0.1622 & 0.2344 & 0.2566 & 0.5767 \\ 0.0999 & 0.1589 & 0.2291 & 0.2449 & 0.5553 \\ 0.1152 & 0.2059 & 0.2637 & 0.3222 & 0.6065 \\ 0.0999 & 0.1580 & 0.2299 & 0.2455 & 0.5850 \\ 0.1083 & 0.1712 & 0.2507 & 0.2682 & 0.6135 \\ 0.1083 & 0.1633 & 0.2388 & 0.2668 & 0.5807 \\ 0.1130 & 0.1526 & 0.2281 & 0.2511 & 0.5829 \\ 0.1135 & 0.1597 & 0.2293 & 0.2563 & 0.6009 \\ 0.1179 & 0.1570 & 0.2318 & 0.2631 & 0.5850 \\ 0.0861 & 0.1240 & 0.1509 & 0.2044 & 0.3907 \\ 0.0864 & 0.1281 & 0.1587 & 0.2128 & 0.4412 \\ 0.0994 & 0.1522 & 0.2171 & 0.2479 & 0.5441 \\ 0.0985 & 0.1562 & 0.2168 & 0.2531 & 0.5229 \end{array} \right]. \end{array}$$

Note that the values are multiplied by a factor of 1.3 to compensate for underestimation of  $\|\sigma\|$ . Standard error is simply given by  $r = R/2$ .

### Relative trace distances between the reconstructed states

In order to compare the quality of the matrices reconstructed with different tomographic protocols, we have also calculated the relative trace distances for the respective states in each protocols. Here we omitted the JKMW protocol, because it provides the largest error radius. Having three relative distances (for the remaining three protocols) it is possible to visualize the relative distances between the matrices and their error radii on a plane.

$$T = \begin{array}{c} \rho_1 \\ \rho_2 \\ \rho_3 \\ \rho_4 \\ \rho_5 \\ \rho_6 \\ \rho_7 \\ \rho_8 \\ \rho_9 \\ \rho_{10} \\ \rho_{11} \\ \rho_{12} \\ \rho_{13} \\ \rho_{14} \\ \rho_{15} \\ \rho_{16} \\ \rho_{17} \end{array} \begin{array}{ccc} T(\rho_O, \rho_M) & T(\rho_O, \rho_S) & T(\rho_M, \rho_S) \\ \left[ \begin{array}{ccc} 0.1415 & 0.1004 & 0.1203 \\ 0.1462 & 0.0798 & 0.1048 \\ 0.1018 & 0.1130 & 0.1362 \\ 0.1295 & 0.1786 & 0.1967 \\ 0.0818 & 0.1684 & 0.1924 \\ 0.1234 & 0.1176 & 0.0818 \\ 0.0806 & 0.0483 & 0.0990 \\ 0.1155 & 0.1150 & 0.1541 \\ 0.1613 & 0.1245 & 0.0998 \\ 0.1397 & 0.0956 & 0.1404 \\ 0.0590 & 0.0515 & 0.0591 \\ 0.1000 & 0.1074 & 0.0960 \\ 0.0896 & 0.1000 & 0.0998 \\ 0.0688 & 0.0425 & 0.0686 \\ 0.0718 & 0.0790 & 0.0813 \\ 0.1506 & 0.1270 & 0.1311 \\ 0.1576 & 0.1278 & 0.1179 \end{array} \right] \end{array}$$


---

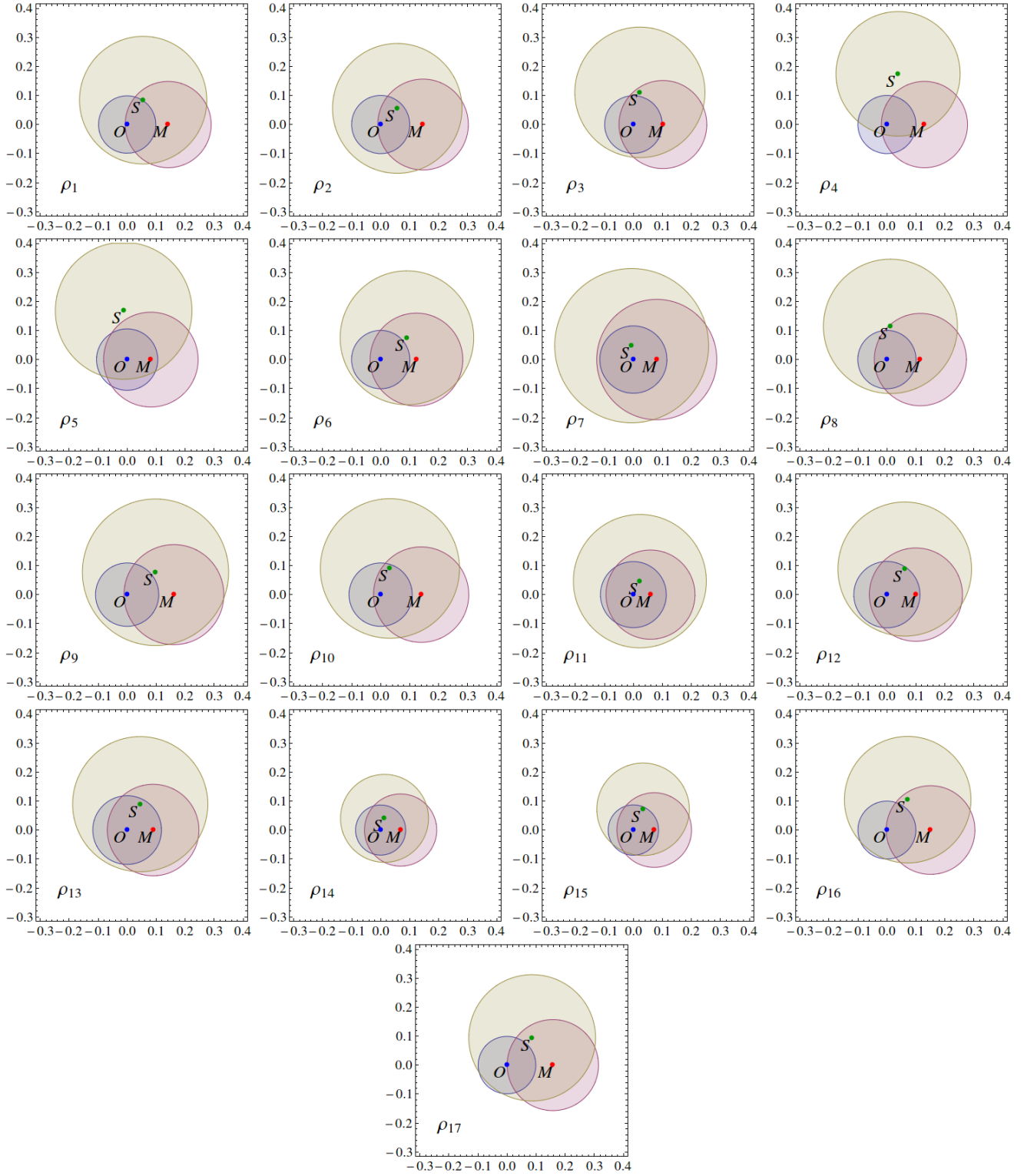


FIG. 4. Relative distances between points representing the reconstructed density matrices and their corresponding circles of the maximum errors  $R$  optimal ( $O$ ), standard ( $S$ ), MUB-based ( $M$ ) tomographies. The 12 states  $\rho_n$  are given in the units of trace distance. The states can be approximated by using Eq. (7) with  $\rho_n = |\psi_n\rangle\langle\psi_n|$ . The absolute positions of the three points are irrelevant. All the states for  $n = 1, \dots, 12$  are fully entangled except  $\rho_7$ . The states of for  $n = 13, \dots, 17$  are partially entangled or separable ( $n = 13, 14$ ). The ideally reconstructed state lies in the intersection of the error circles of radius  $R$ .